Assessing Future Temperature and Precipitation Responses to Solar Radiation Management in Bangladesh: A Comparative Analysis with SSP Scenarios

Afifa Talukder[1], Mohammad Kamruzzaman[2,3], Syed Hafizur Rahman[1,*]

[1]Department of Environmental Sciences, Jahangirnagar University, Savar, Dhaka-1342, Bangladesh; Email: afifatalukdar@gmail.com (AT); hafizsr@juniv.edu (SHR)

[2]Farm Machinery and Postharvest Technology Division, Bangladesh Rice Research Institute, Gazipur 1701, Bangladesh; E-mail: milonbrri@gmail.com

[3]Adjunct Faculty, Dept. of Agrometeorology, Bangabandhu Sheikh Mujibur Rahman Agricultural University (BSMRAU), Salna, Gazipur-1704

*Corresponding author: Syed Hafizur Rahman (hafizsr@juniv.edu)

ORCID: 0000-0003-0112-9124

Abstract

Bangladesh is among the most climate-vulnerable nations globally, facing compounding risks from rising temperatures, shifting precipitation patterns, and intensifying extreme events. This study assesses projected changes in precipitation, maximum temperature (Tmax), and minimum temperature (Tmin) over Bangladesh under two emission pathways — SSP2-4.5 and SSP5-8.5 — and two Solar Radiation Management (SRM) scenarios — G6Solar and G6Sulfur — using bias-corrected CMIP6 multi-model ensemble data for the period 2070–2099. Bias correction using the Quantile Delta Mapping method substantially improved model performance, with Nash-Sutcliffe Efficiency rising from −0.28 to 0.97 for precipitation and from −0.11 to 0.99 for temperature. Relative to the historical baseline (1985–2014), annual Tmax increases by 1.27°C under SSP2-4.5

and 2.36°C under SSP5-8.5, while Tmin increases by 1.71°C and 3.02°C, respectively. SRM scenarios substantially moderate warming, with Tmax increases of 1.33°C (G6Solar) and 1.45°C (G6Sulfur), and Tmin increases of 1.90°C (G6Solar) and 1.95°C (G6Sulfur). Warming is strongest in winter and weakest during the monsoon across all scenarios. Annual precipitation increases across all scenarios relative to historical levels, with the largest rise under SSP5-8.5; however, G6Solar produces 2.5% less precipitation than SSP2-4.5, raising concerns about seasonal drought risk, particularly during pre-monsoon and post-monsoon periods. Spatially, the southeastern and coastal regions experience the greatest increases in both temperature and precipitation, while northern Bangladesh shows comparatively smaller changes. Trend analysis using the Modified Mann-Kendall test reveals significant increasing temperature trends in all scenarios, strongest under SSP5-8.5 (Tmin: 0.47°C decade^{-1}; Tmax: 0.38°C decade^{-1}). The SRM scenarios partially offset high-emission warming but introduce precipitation uncertainties, underscoring that geoengineering should complement, not replace, greenhouse gas mitigation.

Keywords: Geoengineering, GeoMIP6, Climate, CMIP6, Ba

1. Introduction

Bangladesh is one of the countries most vulnerable to the impacts of climate change, experiencing significant challenges as a result of rising temperatures, changing precipitation patterns, and an increase in the frequency and intensity of extreme weather events [1]. With a low-lying geography and a high population density, Bangladesh's exposure to floods, cyclones, sea level rise, and other climate-related disasters makes it particularly susceptible to climate-induced damage [2]. The variability in rainfall and temperature has a direct impact on the country's agriculture, water

resources, biodiversity, and overall socioeconomic stability, posing threats to food security, livelihoods, and public health. Therefore, understanding and potentially mitigating the impacts of climate change is an urgent priority for Bangladesh as it seeks sustainable development and climate resilience [3].

The rise in global temperatures due to greenhouse gas (GHG) emissions has highlighted the need for both mitigation and adaptation measures to address climate impacts. However, the pace of global GHG reduction efforts has been insufficient to keep temperature increases within the 1.5°C or even the 2°C targets set by the Paris Agreement. Consequently, alternative strategies for reducing the impacts of climate change are gaining attention, including Solar Radiation Management (SRM) [4], a form of geoengineering aimed at reflecting a portion of the sun's incoming solar radiation to cool the Earth's surface. SRM techniques, such as stratospheric aerosol injection (SAI), propose injecting reflective particles like sulfate aerosols into the atmosphere (G6Sulfur) [5], or utilizing other solar-shading approaches [6](G6Solar), to counterbalance global warming. These strategies are viewed as potentially effective in reducing global temperatures in the short term; however, the regional effects of SRM interventions remain highly uncertain [7,8].

The regional impacts of SRM, particularly in monsoon-dominated regions like South Asia, have raised concerns about potential unintended consequences. While SRM may reduce global mean temperatures, it may also lead to imbalances in precipitation patterns, as solar radiation plays a significant role in the hydrological cycle [9,10]. For Bangladesh, which relies heavily on the monsoon season for agriculture and water resources, any alteration in seasonal rainfall patterns could have significant adverse effects on food security and the economy. Studies have indicated that SRM could potentially reduce or redistribute rainfall [11–14], with consequences that could either benefit or harm various regions. Understanding these impacts is essential for Bangladesh,

where both too much and too little rainfall have historically resulted in flooding and drought, respectively, with profound impacts on vulnerable communities.

Solar radiation management has been studied across diverse geographical and thematic contexts. In West Africa, stratospheric aerosol injection has been shown to reduce drought severity in the near term, though drought risk may intensify in the far future relative to SSP5-8.5[15]. In Southeast Asia, SRM scenarios have demonstrated potential for reducing hydrological extremes[16], while modeling studies indicate that stratospheric aerosol injection could substantially limit Arctic ice loss depending on injection location and quantity [17]. Agricultural impacts have also been documented, with solar dimming scenarios projected to reduce maize production in China [18]. Despite this growing body of regional evidence, no study has yet examined the effects of SRM on the climatology of Bangladesh — a critical gap given the country's exceptional vulnerability to both temperature and precipitation changes.. The study employs bias-corrected data through the Quantile Delta Mapping (QDM) method to ensure more accurate representations of climate variables, allowing for a detailed examination of changes at the regional scale [19]. Four climate scenarios are examined: two traditional greenhouse gas concentration pathways (SSP2-4.5 and SSP5-8.5) and two SRM intervention scenarios (G6Sulfur and G6Solar). The Shared Socioeconomic Pathway (SSP) scenarios, SSP2-4.5 and SSP5-8.5, provide baseline projections of future temperature and precipitation patterns based on moderate and high levels of greenhouse gas emissions, respectively [20]. The G6Sulfur and G6Solar scenarios introduce SRM interventions into these climate models to assess potential modifications in temperature and precipitation patterns resulting from solar radiation management techniques. The mechanism of SRM is to implement solar radiation management techniques in SSP5-8.5 scenario and achieve reduced

temperature like SSP2-4.5 [4]. The aim of this study is to analyze the regional climatological response of Bangladesh to Solar Radiation Management.

The analysis of SRM's impacts on temperature and precipitation is significant for Bangladesh's climate adaptation strategies, as it will provide policymakers with information on how SRM could influence the country's weather patterns under different climate scenarios. If SRM proves effective in stabilizing temperatures without severe adverse impacts on precipitation, it could offer an additional tool for managing climate risks in Bangladesh. However, if SRM were to significantly reduce or redistribute monsoon rainfall, the strategy could exacerbate climate vulnerabilities in the region. Therefore, this research has broader implications for assessing the trade-offs associated with SRM as a geoengineering strategy, with a focus on balancing the potential benefits of temperature stabilization against the risks of altering critical hydrological processes.

Ultimately, this research underscores the need for a cautious approach to SRM implementation, advocating for further study of SRM's localized impacts before any large-scale interventions are considered. This is especially pertinent for countries like Bangladesh, where the stakes associated with changing climate patterns are exceptionally high. In providing an in-depth analysis of SRM's effects on temperature and precipitation under varying future scenarios, this study aims to enhance the scientific understanding of SRM as a potential tool within the broader context of climate adaptation and mitigation.

2. Methodology

2.1 Study Area

Bangladesh, a South Asian country, characterized by a highly diverse environment, rich biodiversity, and complex climate dynamics. Bangladesh is bordered by India on the west, north, and east, Myanmar to the southeast, and the Bay of Bengal to the south (Fig 1). The country's geographical position and low-lying deltaic topography make it particularly vulnerable to climate variability and extreme weather events such as floods, cyclones, and monsoon-driven precipitation [21]. Bangladesh experiences a tropical monsoon climate, with distinct seasonal variations that significantly influence temperature and precipitation patterns. The pre-monsoon (March-May), monsoon (June-September), post-monsoon (October-November), and winter (December-February) seasons impact agricultural productivity, water resources, and livelihoods. The monsoon season contributes around 80% of the annual rainfall, with average annual precipitation ranging from 1,200 mm in the west to over 5,000 mm in the northeastern hill regions [22]. These seasonal rainfall patterns are critical for agricultural productivity but also increase the risk of severe floods, especially in the Ganges-Brahmaputra-Meghna (GBM) delta [23]. Temperature variations in Bangladesh exhibit significant seasonal shifts. During winter, average temperatures range from 10°C to 20°C, with the northern regions experiencing cooler conditions. In the summer and pre-monsoon seasons, temperatures increase considerably, often reaching 35°C to 40°C in the northwestern regions, which experience extreme heat [24]. Coastal and central areas tend to be warmer and more humid, influenced by proximity to the Bay of Bengal.

Fig 1. Study area map of Bangladesh. Showing the spatial distribution of elevation derived from the Shuttle Radar Topography Mission (SRTM) digital elevation model (DEM). The map

illustrates the topographic variation across the country, including the low-lying floodplains and relatively higher elevations in the southeastern and northeastern regions.

2.2 Datasets

2.2.1 Observation Data

In this study, ERA5 reanalysis data serves as the observational dataset for assessing and validating climate model outputs [25,26]. Monthly data on precipitation, maximum temperature, and minimum temperature from 1985 to 2014 were used, providing a high-quality benchmark for evaluating climate patterns over time. This comprehensive ERA5 dataset ensures that this analysis is anchored in reliable, observationally-derived climate variables, enhancing the precision of model validation and bias correction efforts. ERA5 reanalysis data are available at https://www.ecmwf.int/en/forecasts/dataset/ecmwf-reanalysis-v5.

2.2.2 Climate Model Data

This study utilizes four climate models from the Coupled Model Intercomparison Project Phase 6 (CMIP6) to evaluate the impacts of Solar Radiation Management on precipitation and temperature in Bangladesh. Models are listed in Table 1. These models were carefully selected based on the availability of precipitation, maximum temperature, and minimum temperature data for both historical and projected Shared Socioeconomic Pathway (SSP) scenarios along with projected Solar radiation Management (SRM) scenarios. The historical simulations span from 1985 to 2014, aligning with the ERA5

observational period to facilitate accurate comparison and model validation. For the projected period, data from 2070 to 2099 were used, capturing potential climate changes at the end of the 21st century under different emission scenarios. Two emission scenarios SSP2-4.5 and SSP5-8.5 and two geoengineering scenarios G6Sulfur and G6Solar are analyzed in this study. SSP2-4.5 is medium emission scenario whereas SSP5-8.5 is high emission scenario [20]. Geoengineering techniques are applied in high emission scenarios and aims to achieve global temperature like medium emission scenario. G6Sulfur simulates SRM by injecting sulfur dioxide (SO_2) into the stratosphere, which forms sulfate aerosols that reflect sunlight, thereby cooling the Earth's surface. This method aims to mimic the cooling effect observed after large volcanic eruptions but on a controlled, continuous scale to counteract global warming. G6Solar, on the other hand, models SRM by directly reducing the amount of solar radiation reaching the Earth's surface in climate simulations, without introducing aerosols. This approach allows to examine the effects of solar dimming on climate variables [4]. By comparing the historical and future datasets, this study aims to assess the models' representation of current climate variability and analyze how climate variables may shift under future conditions. This approach ensures a comprehensive evaluation of SRM impacts, grounded in robust model and observational data across both present and future timelines. CMIP6 datasets are available at https://esgf-node.ipsl.upmc.fr/search/cmip6-ipsl/.

Table 1. Description of selected models based on availability of variables in target scenarios

SL. No	Model ID	Institution	Resolution (In degree)
1	CNRM.ESM2.1	Centre National de Recherches Météorologiques, France	1.4°×1.4°
2	IPSL.CM6A.LR	Institute of Pierre Simon Laplace (IPSL), France	2.50°×1.27°
3	MPI.ESM1.2.LR	Max Plank Institute for Meteorology, Germany	1.87°×1.86°
4	UKESM1.0.LL	Natural Environment Research Council (NERC) and the Met Office, UK	1.9°×1.3°

2.3 Bias Correction and Performance Evaluation of Bias corrected data

Datasets are statistically bias corrected using Quantile Delta Mapping technique (QDM). For each climate variable, quantile mapping was applied by matching the cumulative distribution function (CDF) of the model output to that of the observational dataset during the historical period [27,28]. This matching process ensures that the statistical properties (such as mean and variance) of the model outputs are adjusted to match observed climate conditions. QDM calculates the "delta" or change factor for each quantile between the historical and projected model data. These deltas are then applied to the observed quantiles to adjust future projections, preserving the future model-projected change while maintaining consistency with the historical observations [29]. After the correction, the adjusted projections reflect both the projected climate changes and the observed historical data characteristics, offering a more accurate basis for analysis of temperature and precipitation under different SRM and SSP scenarios. After bias correction ensemble mean is calculated for each scenario using Arithmetic Mean (AM) method. Finally, performance evaluation of bias corrected and non-corrected data are calculated on the basis of five error index like Root Mean Square Error (RMSE), Kling Gupta Efficiency (KGE), Nash-Sutcliffe efficiency (NSE), R^2 and Mean Error (ME).

2.3.1 Root Mean Square Error (RMSE)

RMSE is calculated by taking the square root of the average of the squared differences between predicted and observed values. It provides a single value that reflects both the variance and bias of

the errors. Unlike the Mean Absolute Error (MAE), RMSE gives more weight to larger errors because the differences are squared before averaging. Therefore, RMSE is sensitive to outliers. A lower RMSE indicates a better fit of the model to the observed data, as it signifies smaller errors [30].

The RMSE is calculated using the following equation:

$$\text{RMSE} = \sqrt{\frac{1}{N}\sum_{i=1}^{N}(S_i - O_i)^2} \quad (1)$$

Where:

S_i = Simulated (historical) data, O_i = Observed data, N = Number of Observations

2.3.2 Nash-Sutcliffe efficiency (NSE)

The Nash-Sutcliffe Efficiency compares the model's predictions against the observed values and the variability of the observed data. It essentially measures the proportion of the observed variance that is explained by the model predictions. Expected value of NSE is 1 or close to 1 [31].

$$\text{NSE} = 1 - \frac{\sum_{i=1}^{N}(S_i - O_i)^2}{\sum_{i=1}^{N}(O_i - \overline{O})^2} \quad (2)$$

Where,

S_i = Simulated data, O_i = Observation data, N = Number of Observations, $\overline{O}$ is the mean Observation.

2.3.3 Kling Gupta Efficiency (KGE)

KGE provides a more comprehensive view of model performance by considering multiple aspects of the model's accuracy. It combines three components: the correlation between observed and simulated values, the relative bias in the mean, and the variability ratio. The KGE is particularly useful because it captures both the systematic and random errors in a model's prediction, offering a more nuanced understanding of model performance. Expected value of KGE is 1 or close to one. Higher KGE value indicates better model performance [32].

$$\begin{aligned} \mathrm{KGE} &= 1 - \sqrt{(r-1)^2 + (\beta-1)^2 + (\gamma-1)^2} \\ \beta &= \frac{\mu_s}{\mu_o} \\ \gamma &= \frac{\sigma_s/\mu_s}{\sigma_o/\mu_o} \end{aligned} \tag{3}$$

Where,

r is the Pearson correlation coefficient between simulations (s) and observations (o), β is the bias ratio, γ is the variability ratio, μ_o is the mean of observation data, μ_s the mean of modeled data, and σ_o is the standard deviation of the observation data. σ_s is the standard deviation simulated data.

2.3.4 Coefficient of Determinants (R^2)

Coefficient of determination is a statistical metric that measures the proportion of the variance in the dependent variable that is predictable from the independent variable(s) in a regression model. It is a widely used measure of how well the model fits the observed data, particularly in the context of linear regression [33].

$$R^2 = 1 - \frac{\sum_{i=1}^{n} (O_i - S_i)^2}{\sum_{i=1}^{n} (O_i - \bar{O})^2} \quad (4)$$

Where,

S_i = Simulated data, O_i = Observation data, N = Number of Observations, $\overline{O}$ is the mean Observation.

2.3.5 Mean Error (ME)

Mean Error reflects the average magnitude and direction of prediction errors. A positive ME suggests that, on average, the model's predictions are higher than the observed values (overestimation), while a negative ME indicates that the model is underestimating on average. If the ME is close to zero, it suggests that the model has little to no systematic bias, although individual predictions may still have errors [30].

$$\mathrm{ME} = \frac{1}{n}\sum_{i=1}^{n} (O_i - S_i) \quad (5)$$

S_i = Simulated data, O_i = Observation data, N = Number of Observations

2.4 Forecasting of Climatic Variables

Spatial changes are represented as percentage differences compared to the historical period across all scenarios, offering a comprehensive view of how conditions vary spatially. This approach allows for a clear comparison of changes in different geographic areas. In contrast, temporal changes are shown using their actual values, which provides a precise measurement of the change over time. These temporal changes are organized into three categories: monthly changes, seasonal variations, and annual fluctuations. This classification helps to better understand the timing and pattern of changes, offering a detailed breakdown of how the variables evolve on different time scales, from shorter-term monthly shifts to long-term annual trends.

2.5 Trend Analysis

Trends in future climatic variables are evaluated using the Modified Mann-Kendall (MMK) test, an enhanced version of the traditional Mann-Kendall test. This methodology is particularly useful for detecting trends in time series data, especially in the presence of serial correlation (autocorrelation). While the Mann-Kendall test is widely employed for identifying monotonic trends, it does not account for the potential influence of autocorrelation in time series data, which can lead to biased results. The Modified Mann-Kendall test addresses this issue by adjusting for serial dependence, thereby providing a more accurate trend analysis. The significance of the detected trend is determined by examining the p-value of the MMK test. Additionally, to quantify the rate of change, Sen's Slope estimator is used, offering a robust measure of the magnitude and direction of the trend over time.

3 Results

3.1 Performance Evaluation of Bias Corrected Data

Table 2 displays the error indices of before and after bias correction of datasets. Five error indices are considered namely root mean square error (RMSE), Nash–Sutcliffe efficiency (NSE), Kling-Gupta efficiency (KGE), correlation of determinants (R^2) and mean error (ME). All the indices showed better results after bias correction for all variables. In case of precipitation, before bias correction, RMSE was 55.18 which decreased to 8, NSE was -0.28 which increased to 0.97, KGE was 0.42 which increased to 0.97, R^2 was 0.28 which increased to 0.97 and ME became 6.04 from -43.87 after bias correction. Similarly, in case of maximum temperature RMSE was 1 which became 0.01, NSE was -0.11 and it became 0.99, KGE was -0.31 which became 0.99, R^2 was 0.11 which became 0.99. ME was 0.32 which became -0.01. In case of minimum temperature after bias correction RMSE, NSE, KGE, R^2, ME became 0.01, 0.99, 0.99, 0.99 and 0 which were previously 1.11, -0.25, 0.32 0.25 and -0.39 before bias correction.

Table 2. Comparison of error indices of bias corrected and bias uncorrected data

	Precipitation		Max Temp		Min Temp	
	Bias Uncorrected	Bias Corrected	Bias Uncorrected	Bias Corrected	Bias Uncorrected	Bias Corrected
RMSE	55.18	8	1	0.01	1.11	0.01
NSE	-0.28	0.97	-0.11	0.99	-0.25	0.99
KGE	0.42	0.97	-0.31	0.99	0.32	0.99
R^2	0.28	0.97	0.11	0.99	0.25	0.99
ME	-43.87	6.04	0.32	-0.01	-0.39	0

Fig 2 depicts spatial distribution of historical climatic variables before and after bias correction. Here, changes are shown compared to ERA5 data. For precipitation (a,b) changes are shown in

281 percentage and in case of minimum and maximum temperature (c,f) absolute changes are shown.
282 For precipitation after bias correction most of the areas over Bangladesh have only 0 to 5% changes
283 compared to ERA5 observation data which was -20% to -45% before bias correction. For
284 maximum temperature after bias correction temperature flocculation is very low which is only 0
285 to 0.5 compared to observation data and so as to minimum temperature, after bias correction the
286 temperature fluctuation ranges from -1 to 0 in most of the areas of Bangladesh except some
287 southern area.

288

289 **Fig 2. Comparison of ensemble mean before and after bias correction**. (a,b) is precipitation,
290 (c,d) is maximum temperature, (e,f) is Minimum Temperature. (a,c,e) is before bias correction
291 and (b,d,f) is after bias correction. Precipitation change is expressed in percentage and
292 temperature is expressed in absolute difference from observation data.

293

294 3.2 Precipitation and Temperature Projection

295 3.2.1 Projection of Monthly Precipitation and Temperature

296 Table 3 shows average precipitation of each month for historical and projection of four emission
297 scenarios. This table shows monthly average change of precipitation in different scenarios. This
298 change is calculated in percentage compared to the historical data. Over all highest increase is
299 observed in SSP5-8.5 scenario. Highest increase of precipitation in SSP2-4.5 scenario is in the
300 month of May, in SSP5-8.5 it is in the month of February. In G6sulfur highest increase is in the
301 month of January and in G6Solar it is in the month of February. Fig 3(a) represents monthly

average precipitation of different scenarios. SSP5-8.5 projects the highest precipitation, while G6Solar shows the lowest increase among all scenarios, falling slightly below SSP2-4.5; G6Sulfur shows intermediate values between the two SSP scenarios.

Table 3. Monthly average precipitation changes under different scenarios

Average Change of Monthly Precipitation (%)					
Month	Hist (mm)	SSP245 (%)	SSP585 (%)	G6Sulfur (%)	G6Solar (%)
Jan	45.05	3.13	6.85	22.31	-20.61
Feb	71.83	-6.68	34.60	14.30	17.67
Mar	100.92	-4.20	2.71	-13.59	-17.82
Apr	94.01	3.82	27.37	12.16	-0.60
May	171.29	35.01	22.41	9.44	-18.91
Jun	296.47	-0.78	1.11	2.26	-3.05
Jul	477.18	-0.60	2.21	0.84	-0.96
Aug	419.39	14.25	20.22	9.57	-4.93
Sep	337.34	12.60	19.54	9.31	-10.72
Oct	206.78	3.74	12.99	8.93	-3.81
Nov	56.40	9.52	-8.14	-16.44	-9.30
Dec	34.69	1.23	-23.88	-24	16.31

Table 4 shows change of maximum temperature in different scenarios. Unlike precipitation, this change is calculated by subtracting historical temperature from projected temperature. Percentage change is not calculated in case of temperature. According to Table 4 average monthly increase of maximum temperature in G6Sulfur is 1.45 ^{0}C and in G6Solar average increase is 1.33 ^{0}C where as in SSP5-8.5 average temperature increase is 2.36 ^{0}C. lowest increase of maximum temperature is found in SSP2-4.5 scenario where maximum temperature increase by 1.27 ^{0}C. In all scenarios highest change is observed in the month of December. In December, maximum temperature in SSP2-4.5 increases by 2.5 ^{0}C, in SSP5-8.5 increases by 4.21 ^{0}C, in G6Sulfur increases by 2.82 ^{0}C and in G6Solar increases by 2.74 ^{0}C. Fig 3(b) represents maximum temperature over months. It is

observed that SSP2-4.5, G6Sulfur and G6Solar has quite similar temperature variation where as SSP5-8.5 has a very drastic increase of temperature.

Table 4. Monthly maximum temperature changes under different scenarios

Average Change of Monthly Max Temp (^{0}C)					
Month	Hist	SSP245	SSP585	G6Sulfur	G6Solar
Jan	24.60	1.91	3.91	2.33	2.36
Feb	27.34	1.55	2.92	1.83	1.44
March	30.42	1.03	2.05	1.03	1.00
April	32.09	1.19	2.14	1.13	0.95
May	32.53	0.92	1.67	1.08	0.79
Jun	32.08	0.76	1.47	1.01	0.71
July	30.62	0.88	1.69	0.81	0.75
Aug	30.26	0.77	1.52	0.82	0.77
Sep	30.09	0.94	1.78	1.01	1.04
Oct	29.42	1.22	2.03	1.47	1.43
Nov	27.66	1.84	2.98	2.10	2.07
Dec	24.72	2.30	4.21	2.82	2.74

Table 5 shows changes of minimum temperature in different scenarios. Like maximum temperature change of minimum temperature is depicted by subtracting historical values from projected values. Compared to maximum temperature overall increase of minimum temperature is high in all scenarios. Average monthly increase of minimum temperature in G6Sulfur scenario is 1.95 ^{0}C and in G6Solar scenario average monthly increase is 1.90 ^{0}C. Highest change is observed under SSP5-8.5 scenario which is 3.02 ^{0}C. Like maximum temperature lowest increase of minimum temperature is found under SSP2-4.5 which is 1.71 ^{0}C. Fig 3(c) represents monthly minimum temperature cycle. It follows the same pattern of maximum temperature.

Fig 3. Monthly historical and projected precipitation (a), Maximum Temperature(b) and (c) Minimum Temperature in SSP2-4.5, SSP5-8.5, G6Sulfur and G6Solar Scenario. Historical data represents time period from 1985-2014 and projection represents time period from 2070-2099.

Table 5. Monthly minimum temperature changes under different scenarios

Average Change of Monthly Min Temp (^{0}C)					
Month	Hist	SSP245	SSP585	G6sulfur	G6solar
Jan	13.14	2.17	4.93	2.69	2.74
Feb	15.29	2.52	4.99	2.86	2.96
March	19.49	2.34	4.01	2.47	2.42
April	23.15	1.70	2.86	1.81	1.78
May	24.96	1.25	1.59	1.19	1.32
Jun	25.66	0.77	0.90	0.74	0.77
July	25.37	0.86	1.08	0.82	0.84
Aug	25.03	0.99	1.34	0.98	0.95
Sep	24.42	1.41	1.86	1.49	1.45
Oct	22.54	1.78	3.09	2.33	2.05
Nov	18.29	2.31	4.62	3.04	2.74
Dec	14.03	2.46	5.08	3.04	2.79

3.2.2 Projection of Seasonal Precipitation and Temperature

Table 6 summarizes the historical seasonal averages and projected changes in precipitation, maximum temperature (Tmax), and minimum temperature (Tmin) under different climate and geoengineering scenarios. The historical seasonal precipitation shows strong seasonal variability. The monsoon season records the highest precipitation (1530.38 mm), followed by the pre-

monsoon (366.21 mm) and post-monsoon (263.17 mm) seasons, while winter receives the lowest precipitation (151.57 mm). Future projections indicate varying precipitation responses across scenarios. In winter, precipitation is projected to slightly decrease under SSP2-4.5 (−1.95%), while moderate increases are projected under SSP5-8.5 (12.96%), G6Sulfur (7.91%), and G6Solar (3.32%). During the pre-monsoon season, precipitation is projected to increase under SSP2-4.5 (16.19%), SSP5-8.5 (18.25%), and G6Sulfur (3.79%), while G6Solar shows a slight decrease (−0.61%). In the monsoon season, precipitation increases across all scenarios, ranging from 5.37% under G6Sulfur to 10.74% under SSP5-8.5. Similarly, during the post-monsoon season, precipitation increases under SSP2-4.5 (4.98%), SSP5-8.5 (8.46%), and G6Sulfur (3.49%), whereas a minor decrease (−0.30%) is projected under G6Solar.

Historical seasonal averages of maximum temperature (Tmax) range from 25.55 °C in winter to 31.67 °C in the pre-monsoon season, indicating the warmest conditions before the monsoon period. Future projections show increases in Tmax across all seasons and scenarios. In winter, Tmax increases by 1.92 °C under SSP2-4.5 and 3.68 °C under SSP5-8.5, while slightly smaller increases are projected under G6Sulfur (2.18 °C) and G6Solar (2.33 °C). During the pre-monsoon season, Tmax increases range from 0.91 °C (G6Sulfur) to 1.95 °C (SSP5-8.5). In the monsoon season, projected increases are relatively lower, varying between 0.82 °C and 1.62 °C. For the post-monsoon season, Tmax increases range from 1.53 °C under SSP2-4.5 to 2.30 °C under SSP5-8.5, with slightly smaller increases under the geoengineering scenarios. The historical seasonal

averages of minimum temperature (Tmin) vary from 14.15 °C in winter to 25.11 °C during the monsoon season. Future projections show consistent increases in Tmin across all seasons. In winter, Tmin increases range from 2.38 °C under SSP2-4.5 to 5.00 °C under SSP5-8.5, while G6Sulfur (2.86 °C) and G6Solar (2.83 °C) show moderate increases. During the pre-monsoon season, Tmin increases vary between 1.76 °C and 2.82 °C across scenarios. In the monsoon season, projected changes are relatively smaller, ranging from 1.00 °C to 1.29 °C. In the post-monsoon season, Tmin increases range from 2.04 °C under SSP2-4.5 to 3.85 °C under SSP5-8.5, with slightly lower increases under the geoengineering scenarios.

Table 6. Seasonal average precipitation changes under different scenarios

Average Change of Seasonal Precipitation (%)					
Season	Hist	SSP2-4.5 (%)	SSP5-8.5 (%)	G6Sulfur (%)	G6Solar (%)
Winter	151.57	-1.95	12.96	7.91	3.32
Pre monsoon	366.21	16.19	18.25	3.79	-0.61
Monsoon	1530.38	6.34	10.74	5.37	1.25
Post monsoon	263.17	4.98	8.46	3.49	-0.30
Average Change of Seasonal Maximum Temperature (^{0}C)					
Winter	25.55	1.92	3.68	2.18	2.33
Pre monsoon	31.67	1.05	1.95	0.91	1.08
Monsoon	30.76	0.84	1.62	0.82	0.91
Post monsoon	28.54	1.53	2.50	1.75	1.79
Average Change of Seasonal Minimum Temperature (^{0}C)					
Winter	14.15	2.38	5.00	2.86	2.83
Pre monsoon	22.53	1.76	2.82	1.83	1.84
Monsoon	25.11	1.01	1.29	1.01	1.00
Post monsoon	20.41	2.04	3.85	2.69	2.40

Compared to maximum temperature, increase of minimum temperature is higher. Like maximum temperature, highest increase of minimum temperature is also in winter season and lowest is in monsoon season. Among all scenarios SSP5-8.5 has highest increase of minimum temperature while SSP2-4.5 has lowest. In every season G6Sulfur and G6Solar significantly limits increase of minimum temperature compared to SSP5-8.5. In SSP5-8.5 winter temperature increases by 5 ^{0}C whereas G6sulfur and G6Solar limits it with in 2.86 ^{0}C and 2.83 ^{0}C respectively. In monsoon temperature increases by 1.29 ^{0}C while G6Sulfur limits within 1.01 ^{0}C and G6Solar limits with 1.00 ^{0}C. Fig. 4 presents seasonal climate projections across all scenarios, consistent with the percentage changes in Table 6. Precipitation (Fig. 4a) is highest under SSP5-8.5 in all seasons, while G6Solar shows the smallest increases and falls slightly below SSP2-4.5 during pre-monsoon and post-monsoon seasons. Both maximum and minimum temperatures (Fig. 4b, c) show strongest warming in winter under SSP5-8.5 (3.68°C and 5.00°C respectively), while G6Sulfur and G6Solar constrain seasonal warming to levels close to SSP2-4.5 across all seasons.

Fig 4. Historical and projected seasonal precipitation (a), Maximum (b) and minimum (c) temperature in SSP2-4.5, SSP5-8.5, G6Sulfur and G6Solar Scenario. Historical data represents time period from 1985-2014 and projection represents time period from 2070-2099.

3.2.3 Projection of Annual Precipitation and Temperature

Compared to historical period precipitation increases in all the scenarios. Highest increase of precipitation is observed in SSP5-8.5 while lowest in G6Sulfur and G6Solar. Both geoengineering scenarios has lower precipitation than SSP scenarios. Compared to SSP2-4.5 G6Sulfur has 2% less precipitation and compared to SSP5-8.5 G6Sulfur has 7% less precipitation. On the other hand,

G6Solar has 2.5% lower precipitation than SSP2-4.5 and 11.5% compared to SSP5-8.5. Fig 5(a). Like precipitation, maximum temperature and minimum temperature increase is highest in SSP5-8.5. Average increase of maximum temperature is 2.36 ^{0}C and increase of minimum temperature is 3.02 ^{0}C in SSP5-8.5. On the other hand, average increase of maximum temperature and minimum temperature is 1.33 ^{0}C and 1.95 ^{0}C under G6Sulfur and 1.45 ^{0}C and 1.90 ^{0}C under G6Solar. Though the target of geoengineering is to achieve the temperature of SSP2-4.5, but in perspective of Bangladesh it might not be fully achieved. Increase of both maximum and minimum temperature is lower in SSP2-4.5 than all other scenarios. Maximum temperature increases by 1.27 ^{0}C and minimum temperature increases by 1.71 ^{0}C in SSP2-4.5. Fig 5(b) and 5(c) represents annual increase of maximum and minimum temperature under each scenario.

Fig 5. Historical and projected annual precipitation (a), Maximum (b) and minimum (c) temperature in SSP2-4.5, SSP5-8.5, G6Sulfur and G6Solar Scenario. Historical period is from 1985-2014 and future period is from 2070-2099.

Fig 6 represents the spatial distribution of precipitation. Fig 6 (a) and (b) represents observation and historical precipitation. Fig 6(c) to (f) represents projection of precipitation under four scenarios. Fig 6(c) represents precipitation under SSP2-4.5 scenario. In most of the areas precipitation increases by 5-10% while some area of south and south-east and west have increase of precipitation from 10-15%. Northern areas have lowest precipitation increase. In these areas precipitation increases by 2-5%. Fig 6(d) represents precipitation projection under SSP5-8.5 scenario. This scenario has highest increase of precipitation among all. South-eastern part

undergoes huge increase of precipitation. In this area precipitation increases by more than 15 %. In central area precipitation increases by 10% to 15%. In the western part precipitation increases by 5% to 10%. Fig 6(e) represents precipitation in G6Sulfur scenario. Increase of precipitation in bit higher compared to SSP2-4.5 but lower than SSP5-8.5. Lowest increase of precipitation is observed in the northern area. In northern area precipitation increase by 0-5%. In rest of the area precipitation increases by 5% to 10%. Fig 6(f) represents G6Solar scenario. Precipitation is lowest in this scenario. Northern area undergoes negative changes that is precipitation decreases. Highest increase of precipitation is observed in the south-eastern part of Bangladesh that is 5% to 10%. Rest of the areas undergoes 2% to 5% changes.

Fig 6. Historical and Projected annual precipitation over Bangladesh. (a) and (b) represents observation and historical precipitation from 1985-2014. (c) and (d) represents SSP2-4.5 and SSP5-8.5 respectively. (e) and (f) represents G6Sulfur and G6Solar respectively. All four projection are from 2070-2099.

Fig 7 represents maximum temperature changes in Bangladesh. Unlike precipitation, these changes are calculated by the difference of historical and projection temperature, not in percentage. Fig 7(a) and (b) represents observation and historical maximum temperature. Historical data represents observation temperature quite perfectly. Fig 7(c) represents SSP2-4.5 scenario. In this scenario temperature is quite uniform all over the country except some south-eastern hilly regions and few areas in north. In these areas temperature increases by 1.5 ^{0}C – 2.5 ^{0}C in major parts of Bangladesh temperature increases by 1 ^{0}C to 1.5 ^{0}C. Fig 7(d) represents SSP5-8.5 scenario. Temperature

increase is highest in this scenario. In northern, southern and south-eastern region temperature increases by more than 2.5 ^{0}C. Rest of the areas mostly undergo changes by 1.5 ^{0}C to 2 ^{0}C. Fig 7 (e) and (f) are geoengineering scenarios. 7 (e) is G6Sulfur and (f) is G6solar. Both of these scenarios follow maximum temperature pattern of SSP2-4.5 except few changes. In northern and southern parts of Bangladesh G6Solar has higher temperature compared to G6Sulfur.

Fig 7. Historical and Projected annual maximum temperature over Bangladesh. (a) and (b) represents observation and historical precipitation from 1985-2014. (c) and (d) represents SSP2-4.5 and SSP5-8.5 respectively. (e) and (f) represents G6Sulfur and G6Solar respectively. All four projection are from 2070-2099.

Fig 8 represents change of minimum temperature in Bangladesh. Like maximum temperature minimum temperature is also calculated by calculating the difference of historical and projected minimum temperature. Historical data is quite good in replicating observation data as represented in Fig 8(a) and (b). Fig 8(c) represents SSP2-4.5 scenario where change of temperature is lowest and almost uniform all over the country. Almost entire country under goes a temperature rise of 1.5 ^{0}C to 2 ^{0}C. Under SSP5-8.5 temperature rise is highest where almost entire area of Bangladesh undergoes a temperature rise of more than 3 ^{0}C. In northern, southern, south-eastern region has temperature rise of more than 3 ^{0}C and some central to north-eastern and south-eastern parts have temperature rise of 2.5 to 3 ^{0}C. Fig 8 (e) and (f) are geoengineering scenarios. Fig 8(e) is G6Sulfur, in this scenario minimum temperature is uniform except some northern, southern, south-eastern region. These regions have increase of temperature by 2 ^{0}C to 2.5 ^{0}C others have increase of 1.5

459 ^{0}C to 2 ^{0}C. Spatially lower area is exposure to higher temperature increase in G6Solar scenario
460 compared to G6Sulfur scenario. Fig 8(f) represents G6Solar scenario where temperature uniformly
461 increase by 1.5 ^{0}C to 2 ^{0}C in most of the areas. In south-eastern and few parts of south have
462 temperature increase by 2 ^{0}C to 2.5 ^{0}C.

463

464 **Fig 8. Historical and Projected annual minimum temperature over Bangladesh.** (a) and (b)
465 represents observation and historical precipitation from 1985-2014. (c) and (d) represents SSP2-
466 4.5 and SSP5-8.5 respectively. (e) and (f) represents G6Sulfur and G6Solar respectively. All four
467 projection are from 2070-2099.

468

469 The increase of minimum temperature is higher than maximum temperature. Among G6Sulfur and
470 G6Solar scenarios, G6Solar reduces minimum temperature slightly more than G6Sulfur, whereas
471 G6Sulfur shows slightly lower maximum temperature increases compared to G6Solar. Both of the
472 scenarios have lower precipitation than SSP2-4.5 but G6Solar has lower precipitation than
473 G6Sulfur.

474 3.3 Uncertainty Analysis

475 Projection uncertainty was assessed using the median and 5th–95th percentile range for annual
476 precipitation, maximum temperature, and minimum temperature across the scenarios in Table 7.
477 The spread of projections indicates notable differences between the SSP scenarios and the
478 geoengineering scenarios (G6Solar and G6Sulfur). For precipitation, SSP5-8.5 shows the widest
479 uncertainty range (1527.1–4942.6 mm), indicating larger variability among models under high-

emission conditions, whereas SSP2-4.5 has a comparatively narrower range (1580.0–4283.5 mm). In contrast, the geoengineering scenarios show slightly reduced spread, with G6Solar (1542.5–4187.5 mm) exhibiting the narrowest range among future scenarios and G6Sulfur (1519.8–4462.6 mm) showing moderate variability. For maximum temperature, the SSP scenarios again display a broader range, particularly SSP5-8.5 (26.44–33.65 °C), while the geoengineering scenarios show slightly narrower spreads (G6Solar 25.51–32.35 °C; G6Sulfur 25.50–32.06 °C), suggesting reduced inter-model variability. A similar pattern is observed for minimum temperature, where SSP5-8.5 (18.67–28.50 °C) presents the largest spread, whereas G6Solar (17.70–27.80 °C) and G6Sulfur (17.77–27.79 °C) exhibit relatively smaller ranges. Overall, the SSP scenarios, especially the high-emission pathway tends to show greater uncertainty, while the geoengineering scenarios demonstrate slightly more constrained projection spreads, particularly for temperature.

Table 7. Uncertainty analysis of precipitation, maximum minimum temperature under different scenarios (median and 5^{th} – 95^{th} percentile).

Scenario	Precipitation (mm)	Maximum Temperature (ºC)	Minimum Temperature (ºC)
Historical	2334.4 (1501.3, 3985.9)	28.28 (23.89, 30.40)	20.74 (15.65, 26.10)
SSP2-4.5	2522.5 (1580.0, 4283.5)	29.73 (25.37, 32.04)	22.51 (17.48, 27.74)
SSP5-8.5	2672.0 (1527.1, 4942.6)	30.86 (26.44, 33.65)	23.88 (18.67, 28.50)
G6Solar	2473.3 (1542.5, 4187.5)	29.86 (25.51, 32.35)	22.67 (17.70, 27.80)
G6Sulfur	2631.1 (1519.8, 4462.6)	29.82 (25.50, 32.06)	22.72 (17.77, 27.79)

Fig 9 presents the probability density functions for annual precipitation, maximum temperature, and minimum temperature, providing a complementary visualization of the projection uncertainties across scenarios. The probability density plots reinforce the findings from the percentile ranges, clearly illustrating the shifts in central tendencies and the degree of spread under different forcing pathways. For annual precipitation (Fig 9a), the probability density distributions show that SSP5-8.5 exhibits the widest spread with a long tail toward higher precipitation values, reflecting the greater inter-model variability reported in Table 7, whereas SSP2-4.5 displays a comparatively narrower and more peaked distribution. The geoengineering scenarios, particularly G6Solar, show distributions that are shifted toward lower precipitation magnitudes with reduced spread, consistent with the narrower uncertainty ranges observed. For annual maximum temperature (Fig 9b), the probability densities reveal a clear separation between scenarios, with SSP5-8.5 showing the most rightward shift and broadest distribution, indicating both higher warming levels and larger uncertainty. In contrast, G6Solar and G6Sulfur exhibit distributions that are shifted leftward with reduced spread, aligning with the narrower 5th–95th percentile ranges and suggesting that solar radiation modification effectively constrains model variability in temperature projections. A similar pattern is observed for annual minimum temperature (Fig 9c), where the SSP5-8.5 distribution is notably wider and shifted toward higher temperatures, while the geoengineering scenarios display more compact distributions centered at lower values. The probability density functions corroborate the uncertainty quantification from the percentile ranges, demonstrating that high-emission pathways (SSP5-8.5) are associated with greater projection uncertainty and more pronounced warming, whereas geoengineering scenarios yield comparatively constrained uncertainty bounds and moderated climate responses across all three variables.

Fig 9. Probability density distributions of (a) annual precipitation, **(b) annual maximum temperature**, and **(c) annual minimum temperature over Bangladesh under different climate scenarios.** The dashed gray line represents the historical period, while colored lines indicate future projections under SSP2-4.5, SSP5-8.5, G6Solar, and G6Sulfur scenarios.

Fig 10 presents violin plots showing the distribution of annual precipitation, maximum temperature, and minimum temperature for the historical period and future scenarios (SSP2-4.5, SSP5-8.5, G6Solar, and G6Sulfur). The precipitation distribution indicates higher variability under future scenarios compared to the historical period, with SSP5-8.5 exhibiting the highest median precipitation and the widest spread, suggesting increased precipitation variability and intensity. The SSP2-4.5 scenario also shows an upward shift relative to the historical period, while the geoengineering scenarios (G6Solar and G6Sulfur) display comparatively lower precipitation distributions than the SSP scenarios, indicating moderated changes under solar radiation management. For temperature, both maximum and minimum temperature distributions shift upward in all future scenarios relative to the historical period, reflecting a clear warming trend. The SSP5-8.5 scenario shows the highest median values and the broadest distributions for both maximum and minimum temperatures, indicating the strongest warming, whereas SSP2-4.5 shows moderate increases. In contrast, the G6Solar and G6Sulfur scenarios exhibit relatively lower median temperatures and narrower distributions compared to the SSP scenarios, suggesting that geoengineering interventions partially offset the projected warming. Collectively, the violin plots corroborate the uncertainty quantification from Table 7 and Fig 9, demonstrating that while SSP5-8.5 drives substantial warming and precipitation increases with considerable model spread, the geoengineering scenarios produce more constrained distributions but with divergent impacts

G6Solar effectively moderates maximum temperature increases but produces precipitation reductions in pre-monsoon and post-monsoon seasons, whereas G6Sulfur shows slightly higher maximum temperature increases but maintains positive precipitation changes across all seasons.

Figure 10. Violin plots showing the distribution of (a) annual precipitation, **(b) annual maximum temperature, and (c) annual minimum temperature over Bangladesh for the historical period and future climate scenarios (SSP2-4.5, SSP5-8.5, G6Solar, and G6Sulfur)**. The violin shapes represent the probability density of the data, while the internal lines indicate the median and interquartile range.

3.4 Trend Analysis

The overall trends of annual precipitation, maximum temperature, and minimum temperature were analyzed using the Modified Mann–Kendall test and Sen's slope (Table 8**)**, with $p < 0.05$ indicating a significant trend. For precipitation, a significant increasing trend is observed under SSP5-8.5 **(**131.8 mm/decade**)** and G6Sulfur **(**66.2 mm/decade**)**, while G6Solar shows a significant decreasing trend (−44.8 mm/decade), and SSP2-4.5 is not significant ($p = 0.0526$). Both maximum and minimum temperatures show significant increasing trends in all scenarios, with maximum temperature increasing fastest under SSP5-8.5 **(**0.38 °C/decade**)** and slowest under G6Sulfur **(**0.12 °C/decade), while minimum temperature rises most under SSP5-8.5 **(**0.47 °C/decade**)** and least under SSP2-4.5 **(**0.21 °C/decade**)**, indicating that minimum temperature is warming faster than maximum.

562 Table 8. Trend analysis of precipitation, maximum minimum temperature per decade under
563 different scenarios.
564

Precipitation		
	p value	Sen's Slope
SSP2-4.5	0.052641	-66.559
SSP5-8.5	4.86E-05	131.8314
G6Sulfur	8.48E-05	66.19024
G6Solar	0.001662	-44.75
Maximum Temperature		
	p value	Sen's Slope
SSP2-4.5	4.91E-22	0.22277
SSP5-8.5	5.09E-28	0.38209
G6Sulfur	4.76E-14	0.11777
G6Solar	3.46E-36	0.25375
Minimum Temperature		
	p value	Sen's Slope
SSP2-4.5	7.50E-49	0.20783
SSP5-8.5	1.10E-64	0.47047
G6Sulfur	6.77E-43	0.25106
G6Solar	8.59E-51	0.22777

565

566 The spatial patterns of these trends are shown in Figs 11–13, where areas of significant increase
567 or decrease correspond closely with the rates quantified in Table 8, highlighting regional
568 variability in precipitation and temperature trends across scenarios. Across all three variables, the
569 SSP5-8.5 scenario represents the most extreme climatic shift, characterized by a significant
570 nationwide increase in annual precipitation (reaching >15 mm/decade in northern and central
571 regions) and a drastic warming trend exceeding 0.65°C/decade, particularly during the winter and
572 post-monsoon seasons. While SSP2-4.5 shows similar but moderate spatial patterns, the SRM
573 scenarios G6Solar and G6Sulfur demonstrate a clear capacity to decouple temperature increases
574 from rising greenhouse gas concentrations. Specifically, the SRM scenarios effectively cool the

map, shifting the temperature trend intensity from the high-warming reds of the SSP scenarios to much lower intensities (blues and light yellows), effectively limiting annual warming to within 0.13–0.25°C/decade. However, the precipitation spatial plots reveal a trade-off; while SRM mitigates the extreme wetness seen in SSP5-8.5, it introduces localized drying trends (red patches) in the pre-monsoon and monsoon seasons, especially under G6Solar. Overall, while SSP scenarios lead to uniform and significant warming across Bangladesh, SRM scenarios successfully stabilize temperature trends at the cost of altering regional precipitation distribution, with G6Sulfur appearing slightly more effective than G6Solar at maintaining a balanced spatial climate profile.

Fig 11. Spatial distribution of projected precipitation trends (mm/decade) across Bangladesh under different climate scenarios. Columns represent annual, pre-monsoon, monsoon, post-monsoon, and winter seasons**,** while rows correspond to SSP2-4.5, SSP5-8.5, G6Solar, and G6Sulfur scenarios**.** Black dots denote areas where trends are statistically significant ($p < 0.05$).

Fig 12. Spatial distribution of projected maximum temperature trends (ºC/decade) across Bangladesh under different climate scenarios. Columns represent annual, pre-monsoon, monsoon, post-monsoon, and winter seasons, while rows correspond to SSP2-4.5, SSP5-8.5, G6Solar, and G6Sulfur scenarios. Black dots denote areas where trends are statistically significant ($p < 0.05$).

Fig 13. Spatial distribution of projected minimum temperature trends (ºC/decade) across Bangladesh under different climate scenarios. Columns represent annual, pre-monsoon,

597 monsoon, post-monsoon, and winter seasons, while rows correspond to SSP2-4.5, SSP5-8.5,
598 G6Solar, and G6Sulfur scenarios. Black dots denote areas where trends are statistically significant
599 ($p < 0.05$).

600

601

602 4. Discussion

603 This study evaluated projected changes in precipitation, maximum temperature (Tmax), and
604 minimum temperature (Tmin) over Bangladesh under two emission pathways — SSP2-4.5 and
605 SSP5-8.5 — and two Solar Radiation Management scenarios — G6Sulfur and G6Solar — for the
606 period 2070–2099. The results demonstrate that the magnitude, seasonal distribution, and spatial
607 pattern of future climate changes are strongly sensitive to both the emission pathway chosen and
608 the type of geoengineering intervention applied. These findings are broadly consistent with
609 regional climate projection studies across South Asia, which have documented strong scenario-
610 dependency in both temperature and precipitation responses to greenhouse gas forcing [1,34].
611 Taken together, the results confirm that while SRM can meaningfully moderate warming, its
612 hydrological consequences are divergent and scenario-specific, making a nuanced, region-focused
613 evaluation essential.

614 4.1 Precipitation Projections

615 Under the SSP scenarios, SSP5-8.5 demonstrates the most dramatic increase in precipitation, with
616 an overall 9.8% rise compared to historical levels, particularly marked in the month of February.
617 This scenario, indicative of a high-emission future, projects increased hydrological extremes,

618 which could result in greater challenges for water management, agricultural planning, and flood
619 risk. In contrast, SSP2-4.5 shows a more moderate increase of 5.9%, with seasonal patterns
620 indicating higher precipitation in the pre-monsoon period. The SSP scenarios illustrate the
621 potential impact of continued emissions growth on the hydrological cycle, with SSP5-8.5
622 significantly amplifying precipitation and increasing vulnerability to extreme events. Multiple
623 studies concluded that precipitation extreme can increase under higher emission scenarios. This
624 manifests in our results as an approximately 9.8% increase in annual precipitation under SSP5-8.5
625 the largest of all scenarios — with the greatest monthly enhancement occurring in February
626 (34.60%) and the strongest seasonal enhancement during the pre-monsoon (18.25%) and monsoon
627 (10.74%) periods. The pre-monsoon enhancement under SSP5-8.5 is particularly notable, as this
628 season already carries flood risk in Bangladesh, and further amplification of pre-monsoon
629 precipitation could exacerbate waterlogging and early-season flooding [35–38].

630 In the geoengineering scenarios, G6Sulfur and G6Solar both aim to stabilize temperature increases
631 but yield divergent outcomes for precipitation. G6Sulfur shows a minimal increase in annual
632 precipitation (2.9%) compared to the SSP2-4.5, with the most substantial increase occurring in the
633 winter months. Conversely, G6Solar shows a reduction in annual precipitation of approximately
634 2.5% relative to SSP2-4.5, primarily in pre- and post-monsoon seasons. These findings suggest
635 that while geoengineering approaches like G6Sulfur and G6Solar may mitigate some temperature
636 increases, they may have unintended consequences for precipitation, with G6Solar potentially
637 exacerbating drought risk by reducing rainfall in critical seasons. Previous studies also indicate
638 that solar radiation management may suppress regional precipitation due to reduced evaporation
639 and weakened monsoon circulation[39–42].

The study reveals notable differences in temperature increases among scenarios, with SSP5-8.5 exhibiting the most substantial rise in both maximum (2.36°C) and minimum (3.02°C) temperatures. The seasonal analysis shows the most pronounced warming during the winter months, suggesting potential adverse impacts on seasonal crops, biodiversity, and energy demand. Additionally, the rise in minimum temperatures under SSP5-8.5, averaging 3.02°C, is particularly concerning, as it may disrupt the natural cooling cycles, leading to heat stress and compounded health risks. Similar projections of stronger warming under high-emission scenarios have been reported across Bangladesh using CMIP6 models [43].

The geoengineering scenarios effectively limit temperature rise, bringing it very close to SSP2-4.5 targets. Under G6Sulfur, the maximum temperature increases by only 1.45°C, while G6Solar shows a slightly lower rise of 1.33°C, nearly matching the SSP2-4.5 trajectory. Although neither scenario perfectly replicates SSP2-4.5, both approaches substantially curb warming compared to SSP5-8.5 for both maximum and minimum temperatures, demonstrating that geoengineering could almost achieve the moderate-emission temperature goals. Previous studies have also reported that SRM interventions can substantially reduce global and regional temperature increases, although uncertainties remain regarding regional climate responses [44–47]

Spatial projections indicate that the northern regions of Bangladesh experience comparatively smaller increases in both precipitation and temperature across all scenarios, whereas the southeastern regions show more pronounced increases. This spatial heterogeneity is consistent with previous studies that reported stronger hydro-climatic variability in the southeastern and coastal parts of Bangladesh due to complex topography and monsoon circulation influences (Islam et al., 2022; IPCC, 2021). Such regional differences highlight the importance of localized climate

adaptation strategies, as southeastern regions may require greater emphasis on flood management, climate-resilient infrastructure, and water resource planning.

Temporal trend analysis using the Modified Mann–Kendall test and Sen's slope estimator reveals statistically significant increasing trends in both maximum and minimum temperatures across all scenarios. The results indicate that SSP5-8.5 exhibits the strongest warming trend, with Sen's slope values of 0.38 °C decade^{-1} for maximum temperature and 0.47 °C decade^{-1} for minimum temperature. In comparison, the geoengineering scenarios (G6Sulfur and G6Solar) show relatively lower warming rates, reflecting the moderating influence of solar radiation management on global and regional temperatures. Similar findings have been reported in previous modeling studies, which indicate that SRM can significantly reduce the rate of temperature increase, although it cannot completely eliminate regional warming trends due to complex climate feedbacks and spatial variability [42,48].

Another notable finding is that minimum temperature increases faster than maximum temperature across all scenarios, indicating enhanced night-time warming. This phenomenon has been documented in several regional climate studies and may lead to increased heat stress, altered ecosystem functioning, and reduced crop productivity [49–51].

The projected changes in precipitation and temperature have important implications for climate resilience planning in Bangladesh, a country highly vulnerable to climate variability and extreme weather events. The SSP5-8.5 scenario, representing a high-emission pathway, indicates substantial increases in both precipitation and temperature extremes, emphasizing the urgent need for global greenhouse gas mitigation to reduce long-term climate risks [1].

In contrast, geoengineering scenarios such as G6Sulfur and G6Solar demonstrate that Solar Radiation Management (SRM) can significantly limit temperature rise, bringing regional temperatures close to those projected under SSP2-4.5. Previous modeling experiments have also shown that stratospheric aerosol injection and solar dimming strategies can effectively reduce global temperature anomalies, although their regional climate responses remain uncertain [52]. However, SRM is associated with potential trade-offs and unintended consequences, particularly for precipitation patterns. In this study, G6Solar shows a reduction in precipitation compared to SSP2-4.5, which may increase the risk of seasonal droughts. Similar reductions in tropical precipitation under solar geoengineering have been reported in several modeling studies, which show that solar radiation reduction or stratospheric aerosol injection can weaken the hydrological cycle and decrease rainfall in some tropical regions [39,53]. Therefore, geoengineering should be considered a complementary strategy rather than a replacement for emissions reductions, and its implementation requires careful evaluation of regional climate impacts and socio-economic implications.

5 Conclusion

Projected climate changes over Bangladesh differ markedly across emission pathways and solar radiation management (SRM) interventions. Under the high-emission SSP5-8.5 scenario, both precipitation and temperature show substantial increases, indicating heightened hydrological variability and stronger thermal stress across the country. In comparison, the SSP2-4.5 scenario produces smaller increases in both variables, demonstrating the moderating effect of reduced greenhouse-gas emissions. The geoengineering scenarios G6Sulfur and G6Solar significantly limit

705 temperature rise and bring projected temperatures close to those simulated under SSP2-4.5,
706 indicating that SRM can partially offset warming associated with high-emission pathways.
707 However, their effects on precipitation are more complex. G6Sulfur generally produces modest
708 increases in rainfall, while G6Solar tends to reduce precipitation in several seasons, which could
709 elevate drought risk during climatically sensitive periods. Spatial patterns further highlight
710 regional disparities in climate response. Northern parts of Bangladesh experience relatively
711 smaller changes in both temperature and precipitation, whereas the southeastern and coastal
712 regions exhibit more pronounced increases. These spatial differences suggest that climate impacts
713 and associated risks will not be uniform across the country, reinforcing the need for region-specific
714 adaptation strategies such as improved flood management, climate-informed agricultural planning,
715 and resilient infrastructure development. The findings emphasize that while SRM scenarios can
716 moderate temperature increases, they do not fully replicate the climate conditions associated with
717 lower-emission pathways and may introduce additional precipitation uncertainties. Consequently,
718 geoengineering should not be considered a substitute for emissions reduction. A balanced climate
719 strategy integrating greenhouse-gas mitigation, cautious evaluation of geoengineering approaches,
720 and targeted adaptation measures will be essential for strengthening climate resilience,
721 safeguarding vulnerable populations, and supporting sustainable development in Bangladesh.

722

723 # References

724

725 1. Masson-Delmotte V, P. Zhai, A. Pirani, S.L. Connors, C. Péan, S. Berger, et al. IPCC,
726 2021: Summary for Policymakers. In: Climate Change 2021: The Physical Science Basis.

Contribution of Working Group I to the Sixth Assessment Report of the Intergovernmental Panel on Climate Change. Climate Change 2021 – The Physical Science Basis. Cambridge University Press; 2021. doi:10.1017/9781009157896.001

2. Ali A. Climate change impacts and adaptation assessment in Bangladesh. Clim Res. 1999;12: 109–116.

3. Chowdhury MA, Hasan MK, Islam SLU. Climate change adaptation in Bangladesh: Current practices, challenges and the way forward. Journal of Climate Change and Health. Elsevier Masson s.r.l.; 2022. doi:10.1016/j.joclim.2021.100108

4. Kravitz B, Robock A, Tilmes S, Boucher O, English JM, Irvine PJ, et al. The Geoengineering Model Intercomparison Project Phase 6 (GeoMIP6): Simulation design and preliminary results. Geosci Model Dev. 2015;8: 3379–3392. doi:10.5194/gmd-8-3379-2015

5. Pope FD, Braesicke P, Grainger RG, Kalberer M, Watson IM, Davidson PJ, et al. Stratospheric aerosol particles and solar-radiation management. Nature Climate Change. 2012. pp. 713–719. doi:10.1038/nclimate1528

6. Alpert P, Kishcha P, Kaufman YJ, Schwarzbard R. Global dimming or local dimming?: Effect of urbanization on sunlight availability. Geophys Res Lett. 2005;32: 1–4. doi:10.1029/2005GL023320

7. Heyen D, Wiertz T, Irvine PJ. Regional disparities in SRM impacts: the challenge of diverging preferences. Clim Change. 2015;133: 557–563. doi:10.1007/s10584-015-1526-8

8. Yu X, Moore JC, Cui X, Rinke A, Ji D, Kravitz B, et al. Impacts, effectiveness and regional inequalities of the GeoMIP G1 to G4 solar radiation management scenarios. Glob Planet Change. 2015;129: 10–22. doi:10.1016/j.gloplacha.2015.02.010

9. Wang J, Zhang Z, Crabbe MJC, Das LC. Responses of Extreme Climates in South Asia under a G6sulfur Scenario of Climate Engineering. Atmosphere (Basel). 2023;14. doi:10.3390/atmos14101490

10. Narenpitak P, Kongkulsiri S, Tomkratoke S, Sirisup S. Regional impacts of solar radiation modification on surface temperature and precipitation in Mainland Southeast Asia and the adjacent oceans. Sci Rep. 2024;14: 22713. doi:10.1038/s41598-024-73149-6

11. Crook JA, Jackson LS, Osprey SM, Forster PM. A comparison of temperature and precipitation responses to different earth radiation management geoengineering schemes. J Geophys Res. 2015;120: 9352–9373. doi:10.1002/2015JD023269

12. Ji D, Fang S, Curry CL, Kashimura H, Watanabe S, Cole J, et al. Extreme temperature and precipitation response to solar dimming and stratospheric aerosol geoengineering. Atmos Chem Phys. 2018;18: 10133–10156. doi:10.5194/acp-18-10133-2018

13. Irvine PJ, Ridgwell A, Lunt DJ. Assessing the regional disparities in geoengineering impacts. Geophys Res Lett. 2010;37: 1–6. doi:10.1029/2010GL044447

14. Tew YL, Tan ML, Liew J, Chang CK, Muhamad N. A review of the effects of solar radiation management on hydrological extremes. IOP Conference Series: Earth and Environmental Science. Institute of Physics; 2023. doi:10.1088/1755-1315/1238/1/012030

15. Alamou AE, Obada E, Biao EI, Josuézandagba EB, Da-Allada CY, Bonou FK, et al. Impact of Stratospheric Aerosol Geoengineering on Meteorological Droughts in West Africa. Atmosphere (Basel). 2022;13. doi:10.3390/atmos13020234

16. Tan ML, Juneng L, Kuswanto H, Do HX, Zhang F. Impacts of Solar Radiation Management on Hydro-Climatic Extremes in Southeast Asia. Water (Switzerland). 2023;15. doi:10.3390/w15061089

17. Goddard PB, Kravitz B, MacMartin DG, Visioni D, Bednarz EM, Lee WR. Stratospheric Aerosol Injection Can Reduce Risks to Antarctic Ice Loss Depending on Injection Location and Amount. Journal of Geophysical Research: Atmospheres. 2023;128. doi:10.1029/2023JD039434

18. Xia L, Robock A, Cole J, Curry CL, Ji D, Jones A, et al. Solar radiation management impacts on agriculture in China: A case study in the Geoengineering Model Intercomparison Project (GeoMIP). J Geophys Res. 2014;119: 8695–8711. doi:10.1002/2013JD020630

19. Lehner F, Nadeem I, Formayer H. Evaluating skills and issues of quantile-based bias adjustment for climate change scenarios. Adv Stat Climatol Meteorol Oceanogr. 2023;9: 29–44. doi:10.5194/ascmo-9-29-2023

20. O'Neill BC, Tebaldi C, Van Vuuren DP, Eyring V, Friedlingstein P, Hurtt G, et al. The Scenario Model Intercomparison Project (ScenarioMIP) for CMIP6. Geosci Model Dev. 2016;9: 3461–3482. doi:10.5194/gmd-9-3461-2016

21. MoEF. Bangladesh Climate Change Strategy and Action Plan 2009. 2009.

788 22. Shahid S. Rainfall variability and the trends of wet and dry periods in Bangladesh.
789 International Journal of Climatology. 2010;30: 2299–2313. doi:10.1002/joc.2053

790 23. Mirza MMQ. Climate change, flooding in South Asia and implications. Regional
791 Environmental Change. 2011;11: 95–107.

792 24. Shahid S, Harun S Bin, Katimon A. Changes in diurnal temperature range in Bangladesh
793 during the time period 1961-2008. Atmos Res. 2012;118: 260–270.
794 doi:10.1016/j.atmosres.2012.07.008

795 25. Jamal K, Li X, Chen Y, Rizwan M, Khan MA, Syed Z, et al. Bias correction and
796 projection of temperature over the altitudes of the Upper Indus Basin under CMIP6
797 climate scenarios from 1985 to 2100. Journal of Water and Climate Change. 2023;14:
798 2490–2514. doi:10.2166/wcc.2023.180

799 26. Carvalho D, Cardoso Pereira S, Rocha A. Future surface temperatures over Europe
800 according to CMIP6 climate projections: an analysis with original and bias-corrected data.
801 Clim Change. 2021;167. doi:10.1007/s10584-021-03159-0

802 27. Cannon AJ, Sobie SR, Murdock TQ. Bias correction of GCM precipitation by quantile
803 mapping: How well do methods preserve changes in quantiles and extremes? J Clim.
804 2015;28: 6938–6959. doi:10.1175/JCLI-D-14-00754.1

805 28. Cannon AJ. Multivariate Bias Correction of Climate Model Output: Matching Marginal
806 Distributions and Intervariable Dependence Structure. Journal of Climate. 2016;29: 7045–
807 7064. doi:10.1175/JCLI-D-15-0679.s1

808 29. Kim S, Joo K, Kim H, Shin JY, Heo JH. Regional quantile delta mapping method using
809 regional frequency analysis for regional climate model precipitation. J Hydrol (Amst).
810 2021;596. doi:10.1016/j.jhydrol.2020.125685

811 30. Chai T, Draxler RR. Root mean square error (RMSE) or mean absolute error (MAE)? -
812 Arguments against avoiding RMSE in the literature. Geosci Model Dev. 2014;7: 1247–
813 1250. doi:10.5194/gmd-7-1247-2014

814 31. Mccuen RH, Knight Z, Cutter AG. Evaluation of the Nash-Sutcliffe Efficiency Index.
815 Journal of Hydrologic Engineering. 2006;11. doi:10.1061/ASCE1084-0699200611:6597

816 32. Kling H, Author F, Gupta Order of Authors H V, Gupta H V, Yilmaz KK, Martinez-
817 Baquero GF, et al. Decomposition of the mean squared error and NSE performance
818 criteria: Implications for improving hydrological modelling. J Hydrol (Amst). 2009;377:
819 80–91. Available: https://ntrs.nasa.gov/search.jsp?R=20090027858

820 33. Nakagawa S, Johnson PCD, Schielzeth H. The coefficient of determination R2 and intra-
821 class correlation coefficient from generalized linear mixed-effects models revisited and
822 expanded. J R Soc Interface. 2017;14. doi:10.1098/rsif.2017.0213

823 34. Gleckler PJ, Taylor KE, Doutriaux C. Performance metrics for climate models. Journal of
824 Geophysical Research: Atmospheres. 2008;113. doi:10.1029/2007JD008972

825 35. IPCC. IPCC Sixth Assessment Report. 2021. Available: https://www.ipcc.ch/assessment-
826 report/ar6/

827 36. Chen H, Sun J. Significant Increase of the Global Population Exposure to Increased
828 Precipitation Extremes in the Future. Earths Future. 2021;9. doi:10.1029/2020EF001941

829 37. Liu Y, Chen J, Pan T, Liu Y, Zhang Y, Ge Q, et al. Global Socioeconomic Risk of
830 Precipitation Extremes Under Climate Change. Earths Future. 2020;8.
831 doi:10.1029/2019EF001331

832 38. Ge F, Zhu S, Luo H, Zhi X, Wang H. Future changes in precipitation extremes over
833 Southeast Asia: Insights from CMIP6 multi-model ensemble. Environmental Research
834 Letters. 2021;16. doi:10.1088/1748-9326/abd7ad

835 39. Abbas A, Bhatti AS, Ullah S, Ullah W, Waseem M, Zhao C, et al. Projection of
836 precipitation extremes over South Asia from CMIP6 GCMs. J Arid Land. 2023;15: 274–
837 296. doi:10.1007/s40333-023-0050-3

838 40. Nalam A, Bala G, Modak A. Effects of Arctic geoengineering on precipitation in the
839 tropical monsoon regions. Clim Dyn. 2018;50: 3375–3395. doi:10.1007/s00382-017-
840 3810-y

841 41. Ferraro AJ, Highwood EJ, Charlton-Perez AJ. Weakened tropical circulation and reduced
842 precipitation in response to geoengineering. Environmental Research Letters. 2014;9.
843 doi:10.1088/1748-9326/9/1/014001

844 42. Jones A, Haywood J, Boucher O. A comparison of the climate impacts of geoengineering
845 by stratospheric SO_2 injection and by brightening of marine stratocumulus cloud.
846 Atmospheric Science Letters. 2011;12: 176–183. doi:10.1002/asl.291

847 43. Robock A, Oman L, Stenchikov GL. Regional climate responses to geoengineering with
848 tropical and Arctic SO_2 injections. Journal of Geophysical Research: Atmospheres.
849 2008;113. doi:10.1029/2008JD010050

850 44. Kamruzzaman M, Wahid S, Shahid S, Alam E, Mainuddin M, Islam HMT, et al. Predicted
851 changes in future precipitation and air temperature across Bangladesh using CMIP6
852 GCMs. Heliyon. 2023;9. doi:10.1016/j.heliyon.2023.e16274

853 45. Dagon K, Schrag DP. Regional Climate Variability Under Model Simulations of Solar
854 Geoengineering. Journal of Geophysical Research: Atmospheres. 2017;122: 12,106-
855 12,121. doi:10.1002/2017JD027110

856 46. Jones AC, Hawcroft MK, Haywood JM, Jones A, Guo X, Moore JC. Regional Climate
857 Impacts of Stabilizing Global Warming at 1.5 K Using Solar Geoengineering. Earths
858 Future. 2018;6: 230–251. doi:10.1002/2017EF000720

859 47. MacMartin DG, Wang W, Kravitz B, Tilmes S, Richter JH, Mills MJ. Timescale for
860 Detecting the Climate Response to Stratospheric Aerosol Geoengineering. Journal of
861 Geophysical Research: Atmospheres. 2019;124: 1233–1247. doi:10.1029/2018JD028906

862 48. MacMartin DG, Kravitz B, Tilmes S, Richter JH, Mills MJ, Lamarque J, et al. The
863 Climate Response to Stratospheric Aerosol Geoengineering Can Be Tailored Using
864 Multiple Injection Locations. Journal of Geophysical Research: Atmospheres. 2017;122.
865 doi:10.1002/2017JD026868

866 49. MacMartin DG, Kravitz B, Keith DW, Jarvis A. Dynamics of the coupled human–climate
867 system resulting from closed-loop control of solar geoengineering. Clim Dyn. 2014;43:
868 243–258. doi:10.1007/s00382-013-1822-9

869 50. Easterling DR, Horton B, Jones PD, Peterson TC, Karl TR, Parker DE, et al. Maximum
870 and Minimum Temperature Trends for the Globe. Science (1979). 1997;277: 364–367.
871 doi:10.1126/science.277.5324.364

872 51. Peng S, Huang J, Sheehy JE, Laza RC, Visperas RM, Zhong X, et al. Rice yields decline
873 with higher night temperature from global warming. Proceedings of the National
874 Academy of Sciences. 2004;101: 9971–9975. doi:10.1073/pnas.0403720101

875 52. Jihan MdAT, Popy S, Kayes S, Rasul G, Maowa AS, Rahman MdM. Climate change
876 scenario in Bangladesh: historical data analysis and future projection based on CMIP6
877 model. Sci Rep. 2025;15: 7856. doi:10.1038/s41598-024-81250-z

878 53. Robock A, Oman L, Stenchikov GL. Regional climate responses to geoengineering with
879 tropical and Arctic SO_2 injections. Journal of Geophysical Research: Atmospheres.
880 2008;113. doi:10.1029/2008JD010050

881 54. Malik A, Nowack PJ, Haigh JD, Cao L, Atique L, Plancherel Y. Tropical Pacific climate
882 variability under solar geoengineering: impacts on ENSO extremes. Atmos Chem Phys.
883 2020;20: 15461–15485. doi:10.5194/acp-20-15461-2020

884

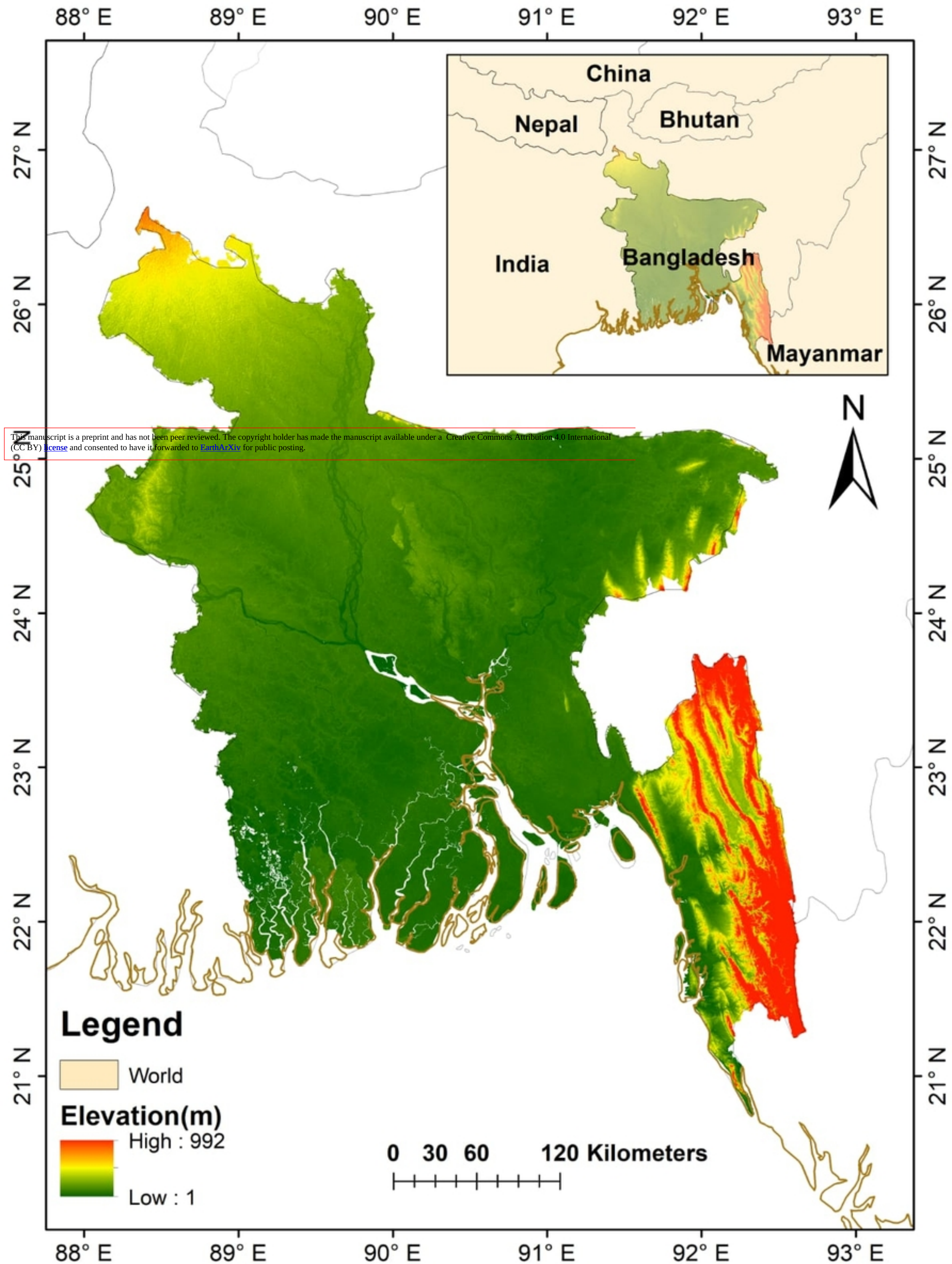

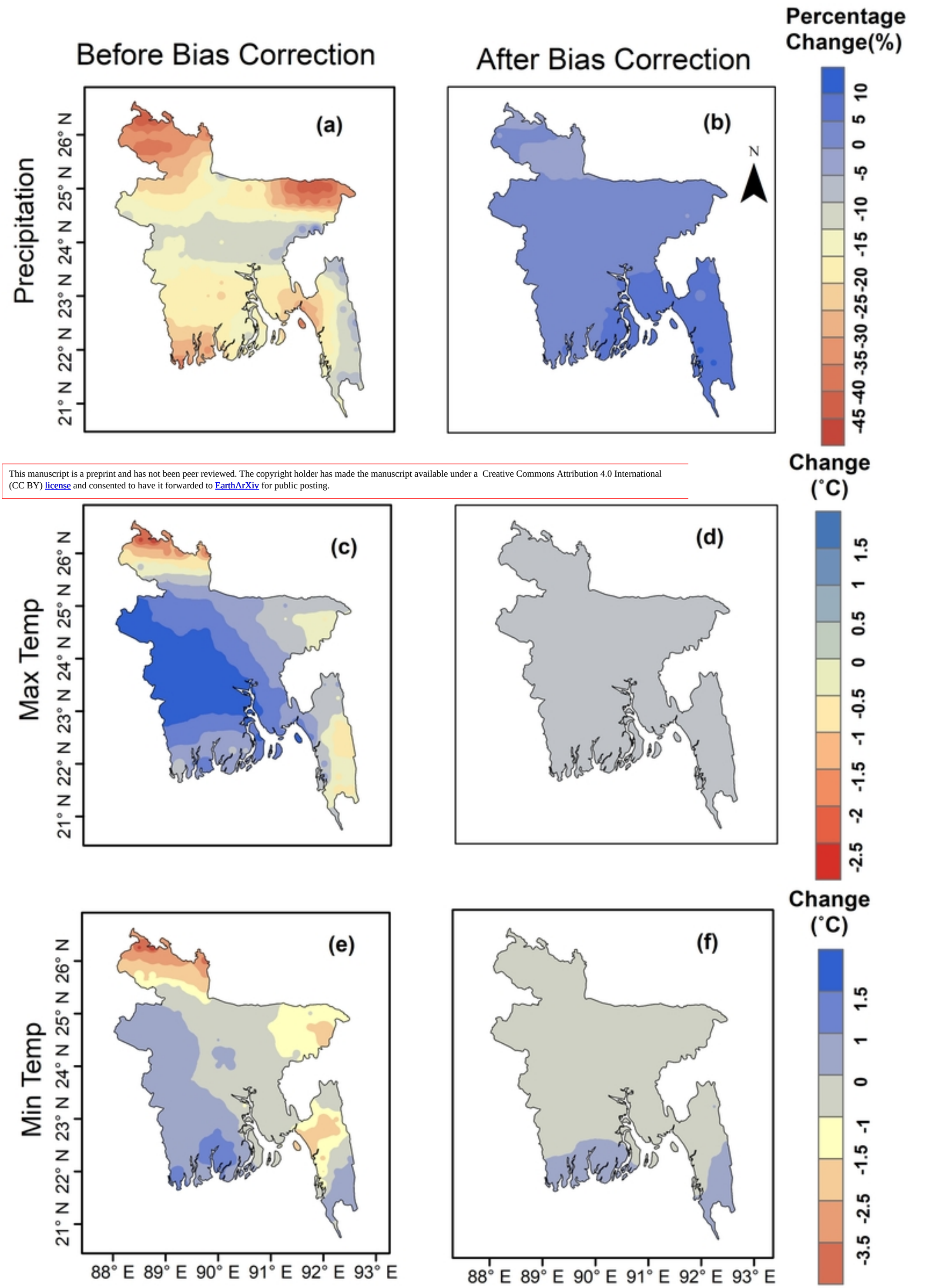

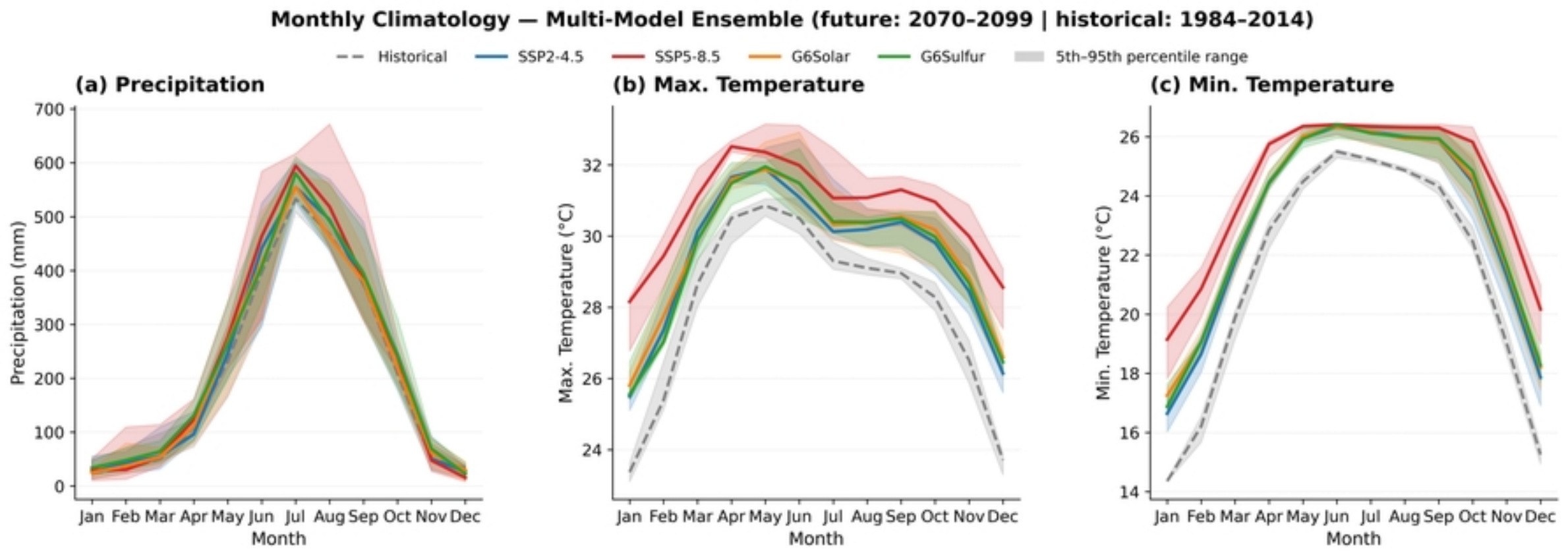
Monthly Climatology — Multi-Model Ensemble (future: 2070–2099 | historical: 1984–2014)
Historical
SSP2-4.5
SSP5-8.5
G6Solar
G6Sulfur
5th–95th percentile range
(a) Precipitation
Precipitation (mm)
0
100
200
300
400
500
600
700
Jan Feb Mar Apr May Jun Jul Aug Sep Oct Nov Dec
Month
(b) Max. Temperature
Max. Temperature (°C)
24
26
28
30
32
Jan Feb Mar Apr May Jun Jul Aug Sep Oct Nov Dec
Month
(c) Min. Temperature
Min. Temperature (°C)
14
16
18
20
22
24
26
Jan Feb Mar Apr May Jun Jul Aug Sep Oct Nov Dec
Month

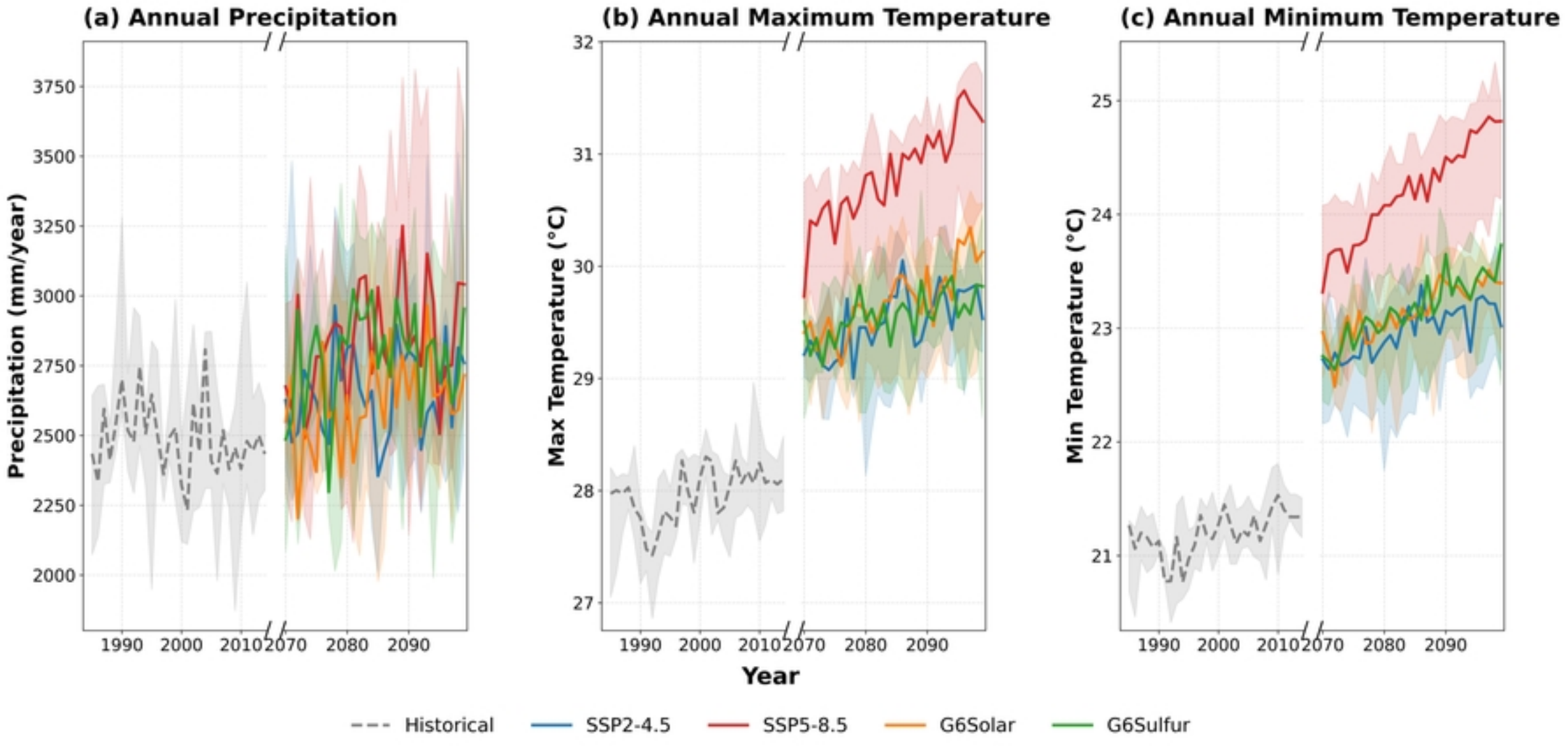
(a) Annual Precipitation
Precipitation (mm/year)
3750
3500
3250
3000
2750
2500
2250
2000
1990
2000
2010
2070
2080
2090
(b) Annual Maximum Temperature
Max Temperature (°C)
32
31
30
29
28
27
(c) Annual Minimum Temperature
Min Temperature (°C)
25
24
23
22
21
Year
Historical
SSP2-4.5
SSP5-8.5
G6Solar
G6Sulfur

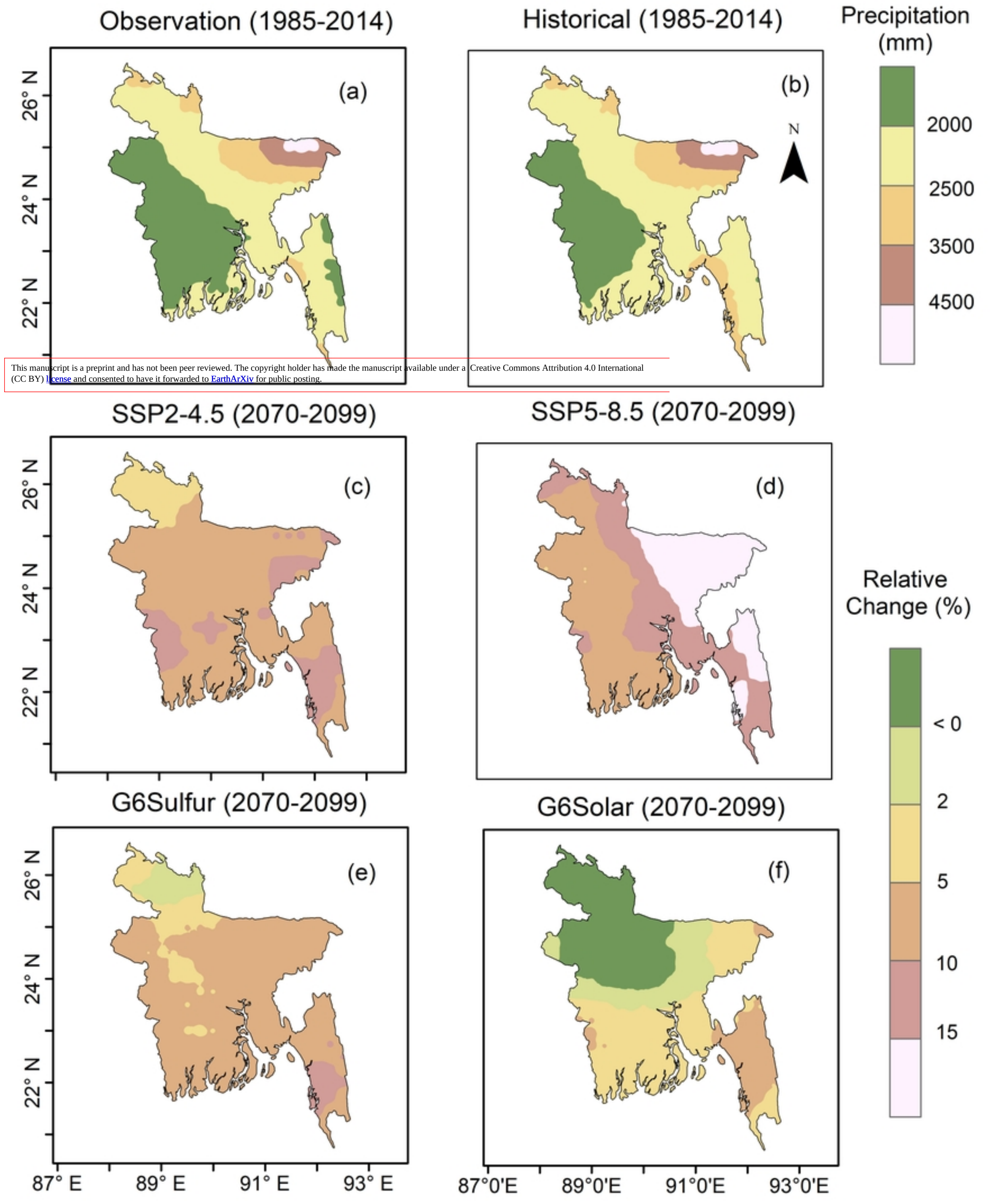

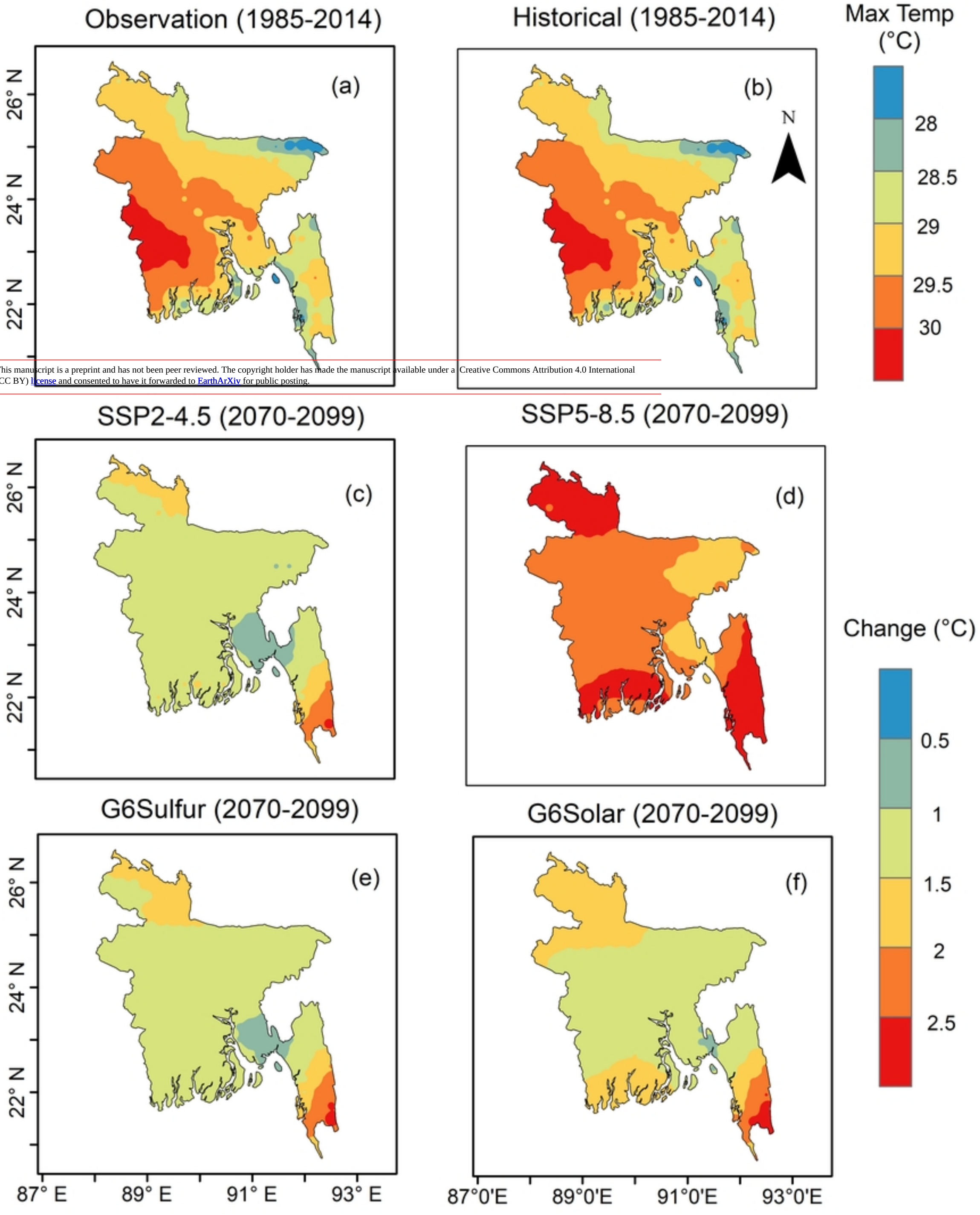

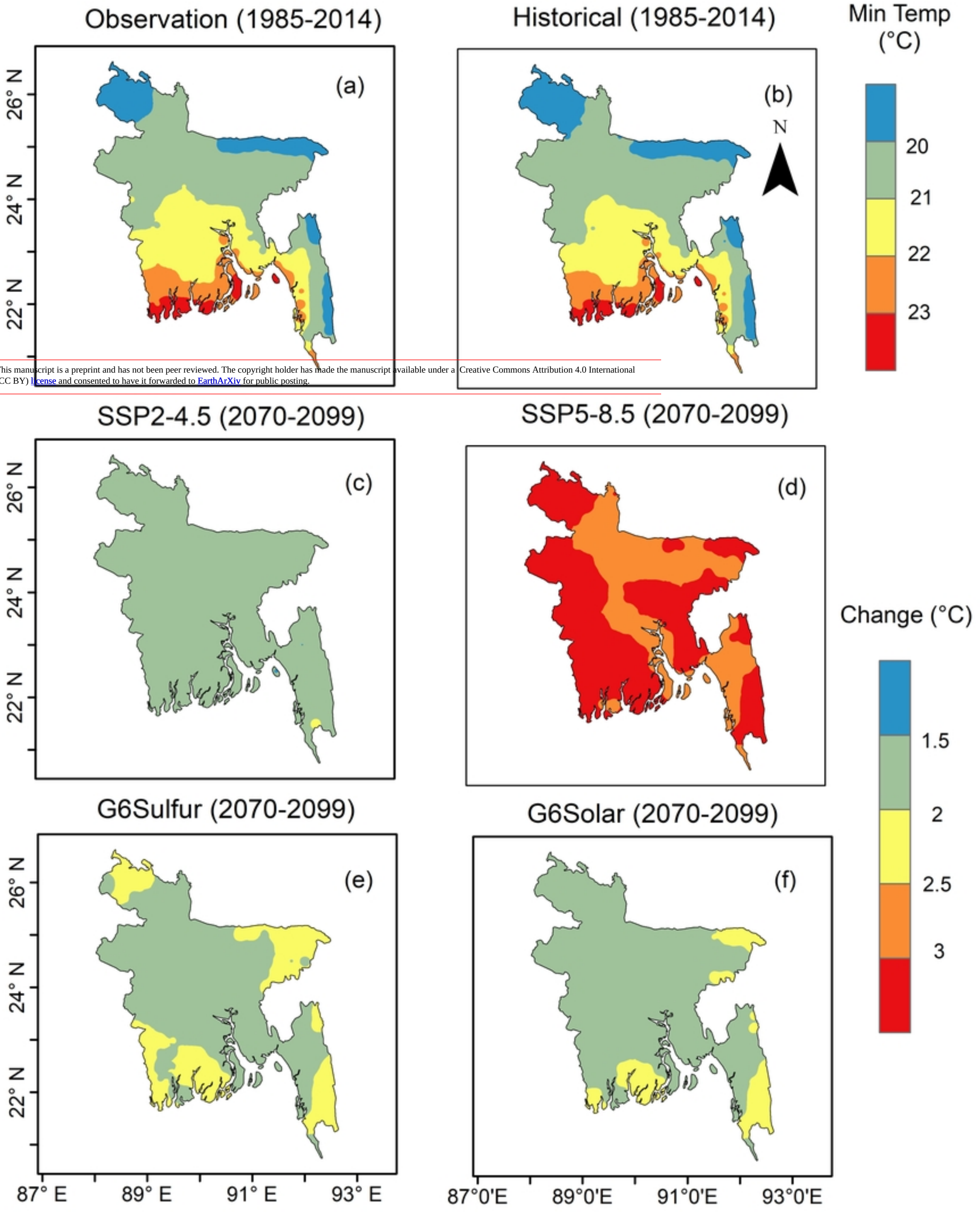

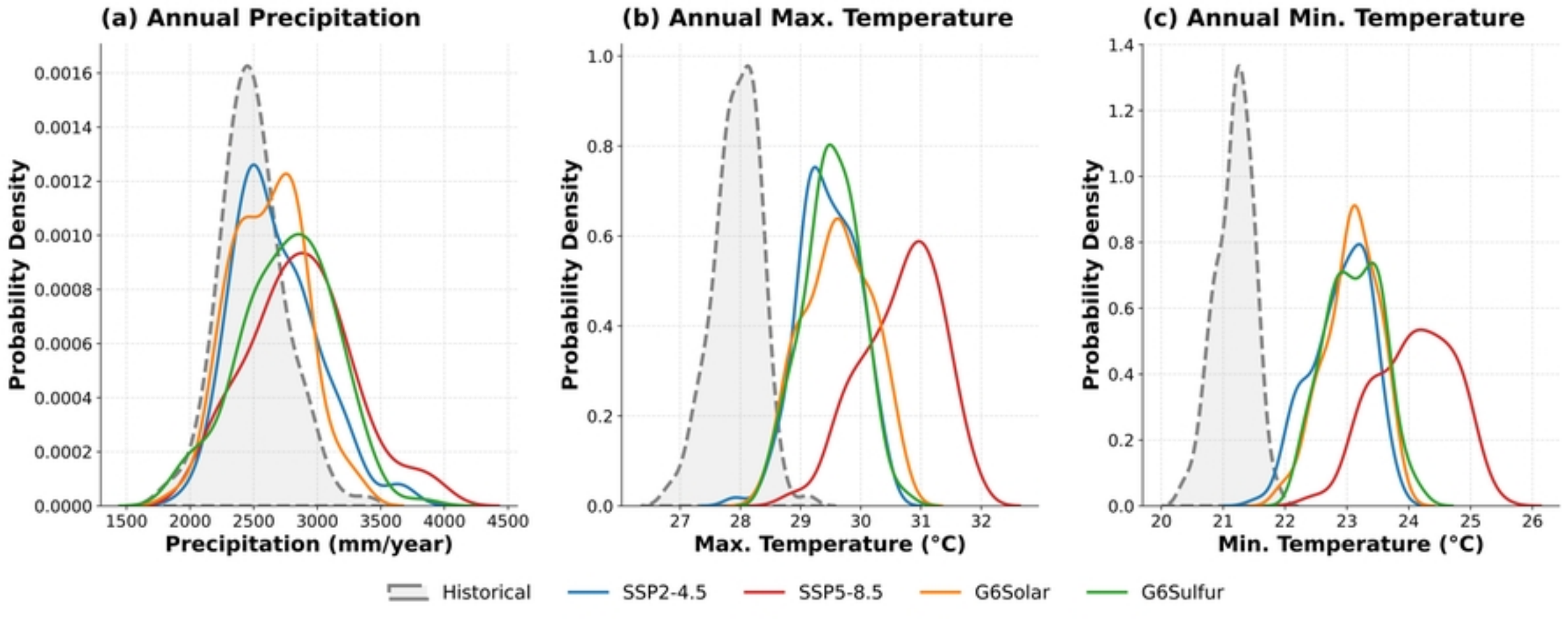
(a) Annual Precipitation
Probability Density
0.0016
0.0014
0.0012
0.0010
0.0008
0.0006
0.0004
0.0002
0.0000
1500
2000
2500
3000
3500
4000
4500
Precipitation (mm/year)
(b) Annual Max. Temperature
Probability Density
1.0
0.8
0.6
0.4
0.2
0.0
27
28
29
30
31
32
Max. Temperature (°C)
(c) Annual Min. Temperature
Probability Density
1.4
1.2
1.0
0.8
0.6
0.4
0.2
0.0
20
21
22
23
24
25
26
Min. Temperature (°C)
Historical
SSP2-4.5
SSP5-8.5
G6Solar
G6Sulfur

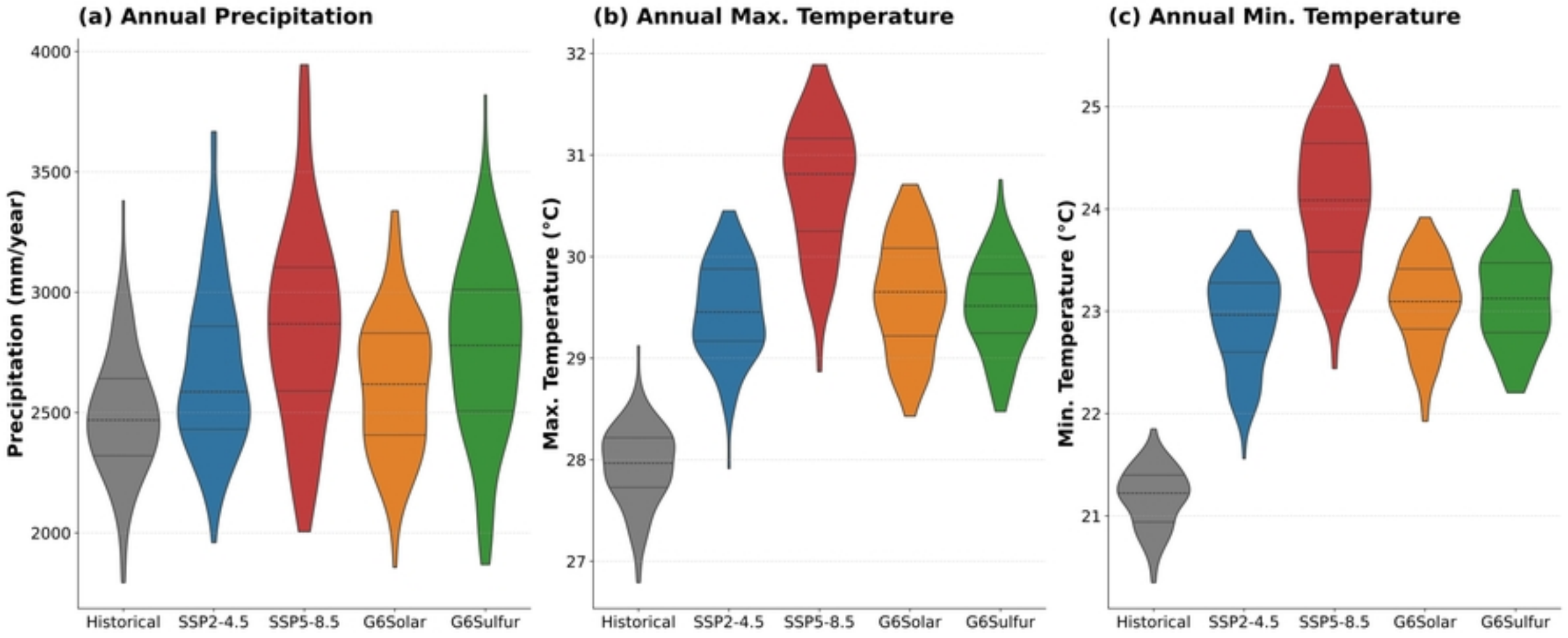
(a) Annual Precipitation
Precipitation (mm/year)
4000
3500
3000
2500
2000
Historical
SSP2-4.5
SSP5-8.5
G6Solar
G6Sulfur
(b) Annual Max. Temperature
Max. Temperature (°C)
32
31
30
29
28
27
Historical
SSP2-4.5
SSP5-8.5
G6Solar
G6Sulfur
(c) Annual Min. Temperature
Min. Temperature (°C)
25
24
23
22
21
Historical
SSP2-4.5
SSP5-8.5
G6Solar
G6Sulfur

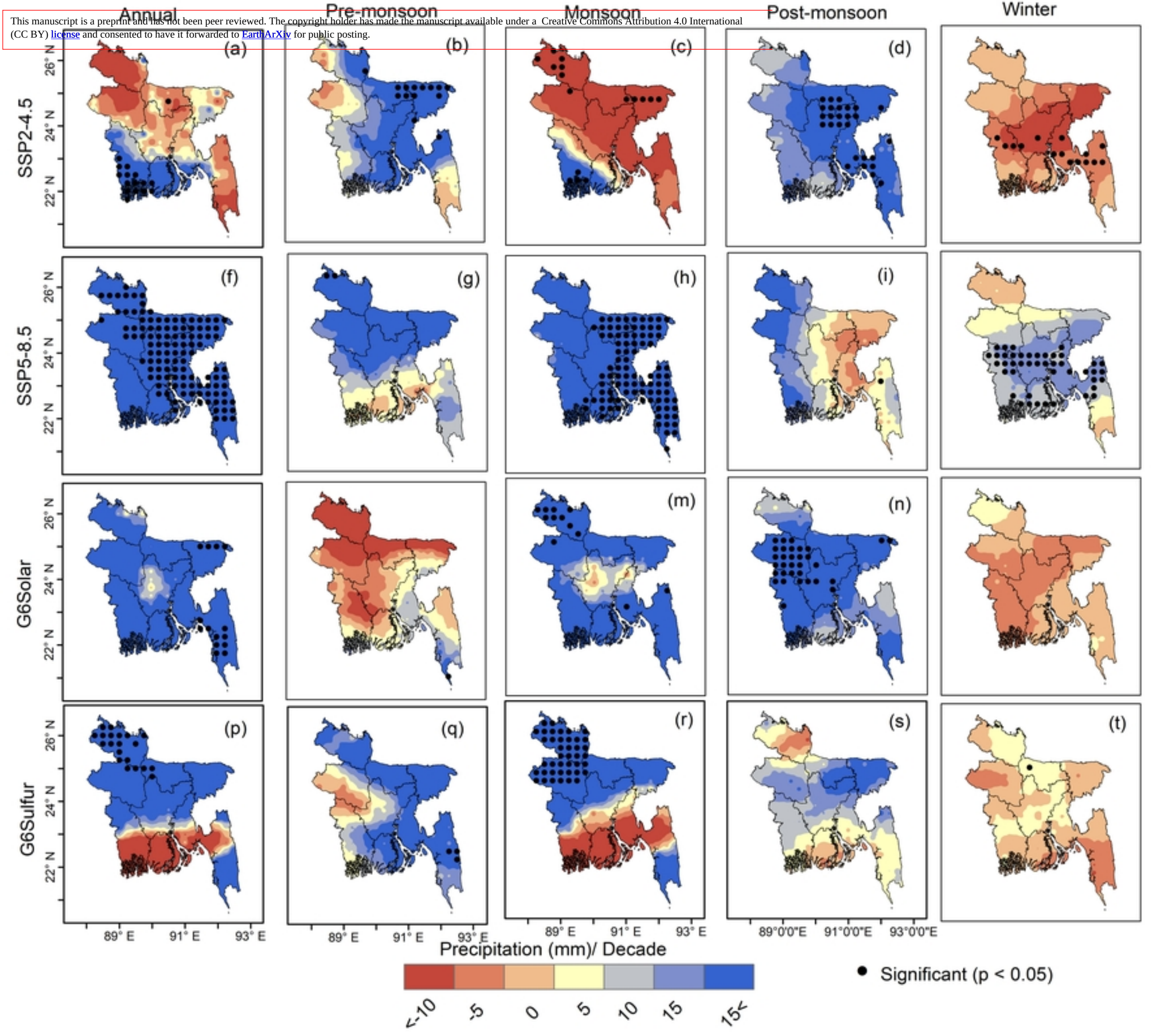

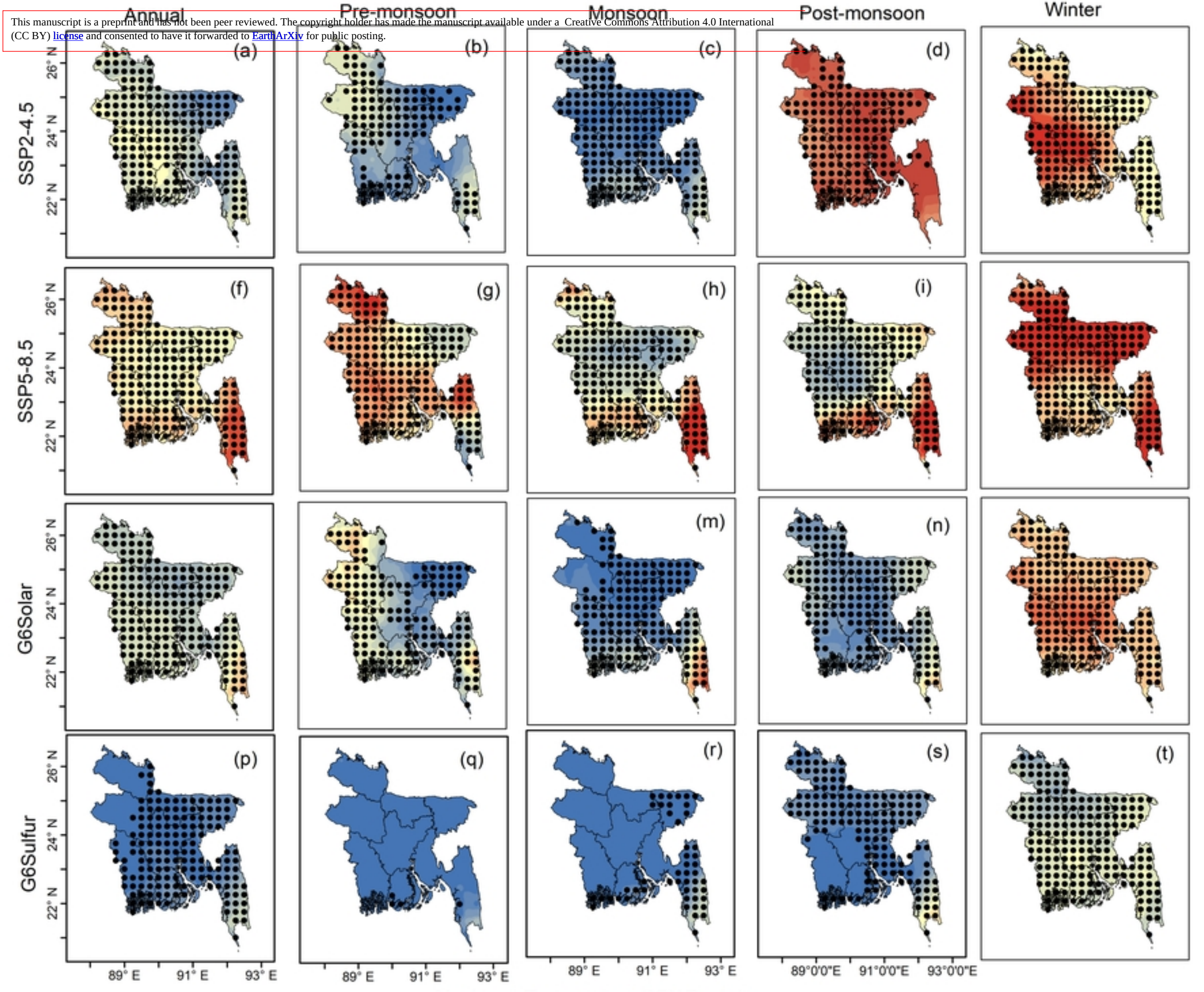

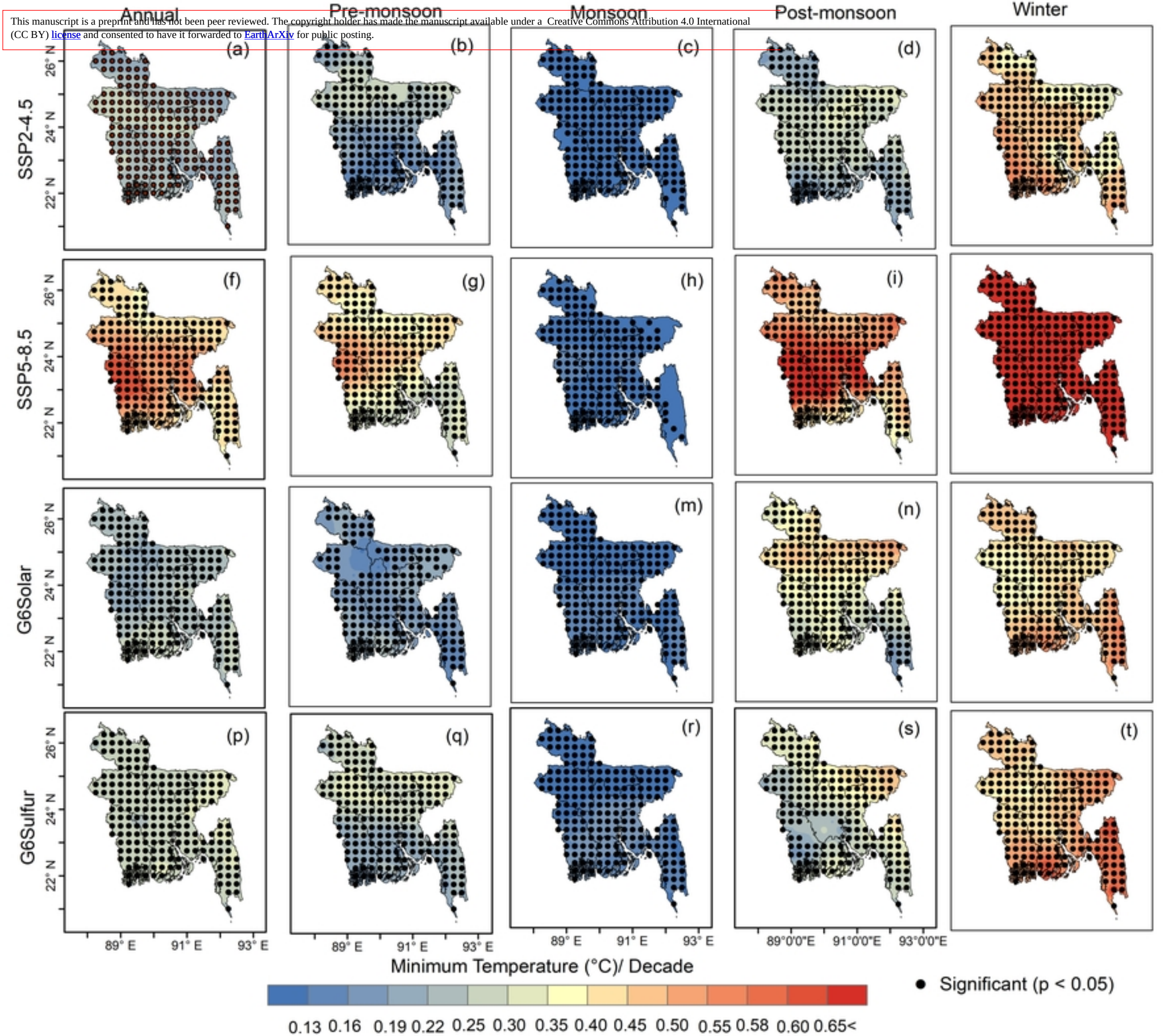

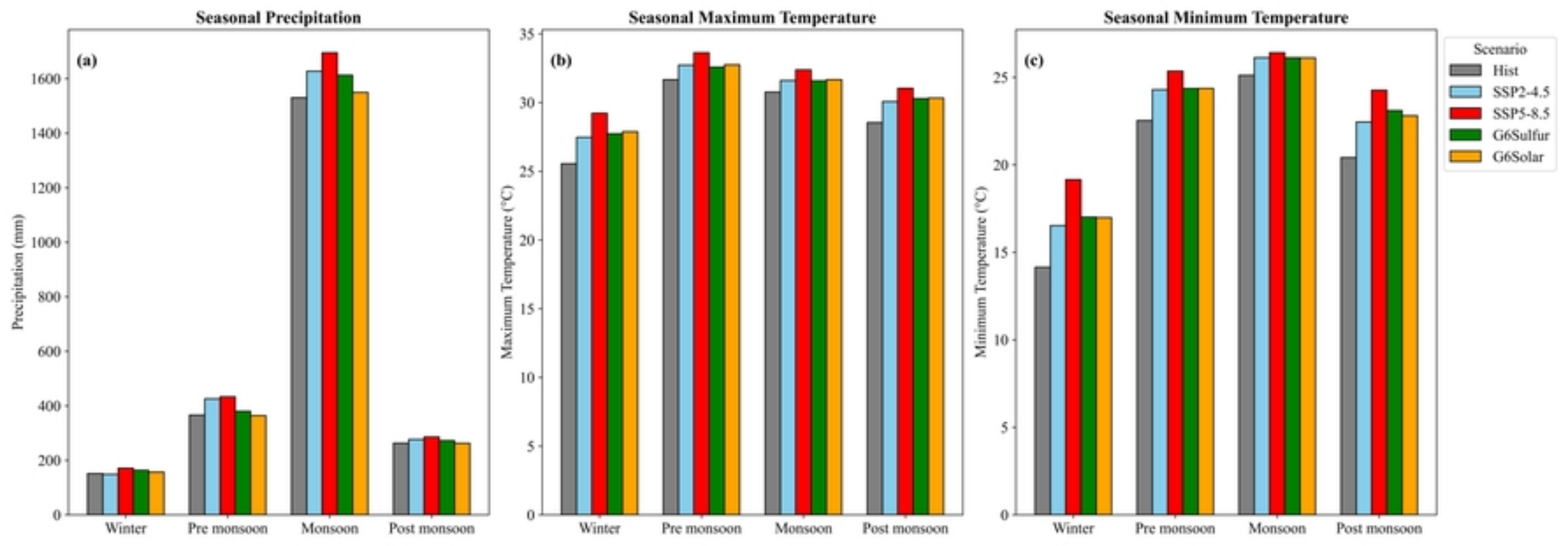
Seasonal Precipitation
(a)
Precipitation (mm)
0
200
400
600
800
1000
1200
1400
1600
Winter
Pre monsoon
Monsoon
Post monsoon
Seasonal Maximum Temperature
(b)
Maximum Temperature (°C)
0
5
10
15
20
25
30
35
Winter
Pre monsoon
Monsoon
Post monsoon
Seasonal Minimum Temperature
(c)
Minimum Temperature (°C)
0
5
10
15
20
25
Winter
Pre monsoon
Monsoon
Post monsoon
Scenario
Hist
SSP2-4.5
SSP5-8.5
G6Sulfur
G6Solar

Figure